Syntheses and Structures of $TcOF_5$ and the $Tc_2O_2F_9^+$ Cation and Formation of the $TcOF_4^+$ Cation in Solution†

Nicolas LeBlond,‡ Hélène P. A. Mercier,‡ David A. Dixon,§ and Gary J. Schrobilgen*,‡

Department of Chemistry, McMaster University, Hamilton, Ontario L8S 4M1, Canada, and Environmental Molecular Sciences Laboratory, Pacific Northwest Laboratory, P.O. Box 999, KI-83, Richland, Washington 99352

Received December 3, 1999

The last member of the series of technetium(VII) oxide fluorides, $TcOF_5$, has been prepared by oxidative fluorination of TcO_2F_3 with KrF_2 in anhydrous HF. The pseudooctahedral (C_{4v}) structure of $TcOF_5$ has been determined by ^{19}F and ^{99}Tc NMR, Raman, and infrared spectroscopies and by single-crystal X-ray diffraction. $TcOF_5$ crystallizes in the orthorhombic crystal system, space group $Pna2_1$, with $a = 9.235(3)$ Å, $b = 4.939(2)$ Å, $c = 8.502(3)$ Å, $V = 387.7(2)$ Å^3, and $Z = 4$ at −102 °C, $R_1 = 0.0256$ and $wR_2 = 0.0730$. $TcOF_5$ behaves as a fluoride ion donor toward AsF_5 and SbF_5 in HF solvent, giving the $Tc_2O_2F_9^+$ cation, which has been characterized as the AsF_6^- and $Sb_2F_{11}^-$ salts by Raman spectroscopy and as the $[Tc_2O_2F_9][Sb_2F_{11}]$ salt by single-crystal X-ray diffraction. $[Tc_2O_2F_9][Sb_2F_{11}]$ crystallizes in the orthorhombic crystal system, space group *Pbcm*, with $a = 6.2925(4)$ Å, $b = 21.205(2)$ Å, $c = 11.7040(8)$ Å, $V = 1561.7(2)$ Å^3, and $Z = 8$ at −90 °C, $R_1 = 0.0368$ and $wR_2 = 0.0896$. The $Tc_2O_2F_9^+$ cation consists of two fluorine-bridged square pyramidal $TcOF_4$ groups in which the fluorine bridge is trans to the oxygens. Solution ^{19}F and ^{99}Tc NMR spectra of $Tc_2O_2F_9^+$ salts in HF and of $TcOF_5$ dissolved in SbF_5 are consistent with the formation of the $TcOF_4^+$ cation. Local density functional theory has been used to calculate the geometrical parameters, vibrational frequencies, and ^{19}F and ^{99}Tc NMR parameters of MOF_5 (M = Tc, Re, Os) and $Tc_2O_2F_9^+$, which are in good agreement with available experimental values. The results of ab initio calculations and normal coordinate analyses for MOF_5 confirm the trans influence of oxygen, which leads to lengthening of the axial fluorine−metal bond length and a correspondingly lower stretching force constant relative to that of the shorter equatorial metal−fluorine bonds.

Introduction

Rhenium oxide pentafluoride, $ReOF_5$, can be prepared relatively easily by high-temperature fluorination of ReO_2 with elemental fluorine,[1] whereas TcO_2 is only fluorinated to TcO_3F under similar conditions.[2] The relative resistance of Tc^{VII} to further fluorination follows the trend of increased oxophilicity in going from Re^{VII} to Tc^{VII} to Mn^{VII} and also dominates osmium(VIII) and ruthenium(VIII) oxide fluoride chemistry.[3] The synthesis and structural characterization of TcO_3F has been described by Selig and co-workers[2,4] and by Schrobilgen and co-workers.[5] Subsequent work from this laboratory has described the synthesis of TcO_2F_3 by reaction of XeF_6 with TcO_3F in HF solvent[6] as well as the fluoride ion acceptor[7] and donor[8] properties of TcO_2F_3. Further fluorination of TcO_2F_3 by XeF_6 in anhydrous HF does not occur.[6]

Detailed structures of the only other known transition metal oxide pentafluorides, $ReOF_5$ and $OsOF_5$, have yet to be determined. On the basis of normal coordinate analyses[9] of the vibrational frequencies of $ReOF_5$ and $OsOF_5$ using generalized valence force fields, it was concluded that the axial M−F bonds are significantly more covalent than the equatorial bonds, and contrast with the lengthening of the axial bond anticipated as a result of the trans influence of the oxo ligand.[7,10−12] A gas-phase electron diffraction study[13] confirmed the expected C_{4v} geometry of $ReOF_5$, but the axial and equatorial Re−F bond lengths were refined as a single parameter and therefore could not be differentiated. The single crystal X-ray structure of $OsOF_5$ has been determined,[14] but distinction between the oxygen and fluorine atoms was not possible because of absorption. As a result, the reported bond lengths are not precise enough to differentiate between axial and equatorial Os−F bond lengths.

† Dedicated to the memory of John G. Malm (June 24, 1921 to May 11, 1999) and his many outstanding contributions to the field of inorganic fluorine chemistry.

‡ McMaster University.

§ Pacific Northwest Laboratory.

(1) Aynsley, E. E.; Peacock, R. D.; Robinson, P. L. *J. Chem. Soc.* **1950**, 1622.
(2) Selig, H.; Malm, J. G. *J. Inorg. Nucl. Chem.* **1963**, *25*, 349.
(3) Gerken, M.; Mercier, H. P. A.; Schrobilgen, G. J. In *Advanced Inorganic Fluorides: Syntheses, Characterization and Applications*; Nakajima T., Tressaud, A., Žemva B., Eds.; Elsevier Sciences S. A.: New York, 1999; Chapter 5.
(4) Binenboym, J.; El-Gad, U.; Selig, H. *Inorg. Chem.* **1974**, *13*, 319.
(5) Franklin, K. J.; Lock, C. J. L.; Sayer, B. G.; Schrobilgen, G. J. *J. Am. Chem. Soc.* **1982**, *104*, 5303.
(6) Mercier, H. P. A.; Schrobilgen, G. J. *Inorg. Chem.* **1993**, *32*, 145.
(7) Casteel, Jr., W. J.; LeBlond, N.; Mercier, H. P. A.; Schrobilgen, G. J. *Inorg. Chem.* **1998**, *37*, 340.
(8) LeBlond, N.; Dixon, D. A.; Schrobilgen, G. J. *Inorg. Chem.* **2000**, *39*, 2473.
(9) Shalabi, A. S.; Nour, E. M. E. *Gazz. Chim. Ital.* **1991**, *121*, 555.
(10) Christe, K. O.; Dixon, D. A.; Mack, H. G.; Oberhammer, H.; Pagelot, A.; Sanders, J. C. P.; Schrobilgen, G. J. *J. Am. Chem. Soc.* **1993**, *115*, 11279.
(11) Casteel, W. J., Jr.; Dixon, D. A.; Mercier, H. P. A.; Schrobilgen, G. J. *Inorg. Chem.* **1996**, *35*, 4310.
(12) Casteel, Jr., W. J.; Dixon, D. A.; LeBlond, N.; Lock, P. E.; Mercier, H. P. A.; Schrobilgen, G. J. *Inorg. Chem.* **1999**, *38*, 2340.
(13) Alekseichuk, I. S.; Ugarov, V. V.; Sokolov, V. B.; Rambidi, N. G. *J. Struct. Chem. (Engl. Transl.)* **1981**, *22*, 795; *Zh. Strukt. Khim.* **1981**, *22*, 182.
(14) Bartlett, N.; Trotter, J. *J. Chem. Soc. A* **1968**, 543.

10.1021/ic991397e CCC: $19.00
Published on Web 09/09/2000

Table 1. Summary of Crystal Data and Refinement Results for $TcOF_5$ and $[Tc_2O_2F_9][Sb_2F_{11}]$

	$TcOF_5$	$[Tc_2O_2F_9][Sb_2F_{11}]$		$TcOF_5$	$[Tc_2O_2F_9][Sb_2F_{11}]$
empirical formula	F_5OTc	$F_{20}O_2Sb_2Tc_2$	mol wt	209.00	425.75
space group	$Pna2_1$ (no. 33)	*Pbcm* (no. 57)	calcd density (g cm^{-3})	3.580	3.622
a (Å)	9.235(3)	6.2925(4)	*T* (°C)	−102	−90
b (Å)	4.939(2)	21.205(2)	μ (mm^{-1})	3.724	5.372
c (Å)	8.502(3)	11.7040(8)	wavelength (Å)	0.710 73	0.710 73
V (Å^3)	387.7(2)	1561.7(2)	final *R* indices [$I > 2\sigma(I)$][a]	$R_1 = 0.0256$	$R_1 = 0.0368$
no. of molecules/unit cell	4	8		$wR_2 = 0.0730$	$wR_2 = 0.0896$

[a] $R_1 = \sum||F_o| - |F_c||/\sum|F_o|$ for $I > 2\sigma(I)$. $wR_2 = [\sum[w(F_o^2 - F_c^2)^2]/\sum w(F_o^2)^2]^{1/2}$ for $I > 2\sigma(I)$.

The fluoride ion donor behavior of $ReOF_5$ toward the strong Lewis acids AsF_5 and SbF_5 has been studied,[15] resulting in salts of the $Re_2O_2F_9^+$ and $ReOF_4^+$ cations. The structure of the binuclear $Re_2O_2F_9^+$ cation was determined by X-ray crystallography as its $Sb_2F_{11}^-$ salt and consists of two fluorine-bridged $ReOF_5$ units with the oxo ligands trans to the bridging fluorine. The compound resulting from the combination of $ReOF_5$ and AsF_5 was described as $[ReOF_4][AsF_6]$ on the basis of the 1:1 combining ratio of $ReOF_5$ and AsF_5, the mass spectrum, and the Raman spectrum. Although the bands attributed to the $ReOF_4^+$ cation in the Raman spectrum of $ReOF_5 \cdot AsF_5$ are similar in frequency and relative intensity to those of $[Re_2O_2F_9][Sb_2F_{11}]$, they correlate well with the infrared spectra of the isovalent monomers $MoOF_4$ and WOF_4[16] and that of the $ReOF_4$ monomer,[17] which have square pyramidal geometries in the gas phase.

An earlier communication from this laboratory provided a preliminary account of the synthesis and structural characterization of the last member of the technetium(VII) oxide fluoride series, $TcOF_5$, by Raman and NMR spectroscopies.[18] The present paper details the synthesis of $TcOF_5$ and its full characterization in solution by ^{19}F and ^{99}Tc NMR and Raman spectroscopy, in the solid state by Raman spectroscopy and X-ray crystallography, and in the gas phase by infrared spectroscopy. The fluoride-ion donor behavior of $TcOF_5$ toward the strong fluoride ion acceptors AsF_5 and SbF_5 is also examined, leading to the detailed structural characterization of the novel $Tc_2O_2F_9^+$ cation and the characterization of $TcOF_4^+$ in solution. An attempt to prepare the TcF_6^+ cation is also described.

Results and Discussion

Technetium Oxide Pentafluoride. (a) Synthesis of $TcOF_5$. No evidence was found for the fluorination of TcO_2F_3 to $TcOF_5$ when TcO_3F was fluorinated to TcO_2F_3 in anhydrous HF using excess XeF_6. Instead, excess XeF_6 present in these systems acts as a fluoride ion donor, solubilizing TcO_2F_3 to form $[XeF_5][TcO_2F_4]$.[6] In an attempt to produce a stronger fluorinating

$$TcO_2F_3 + 2XeF_6 \xrightarrow{XeF_6,\ 35\ °C} [Xe_2F_{11}][TcO_2F_4] \qquad (1)$$

medium, TcO_2F_3 was dissolved in an 8-fold molar excess of molten XeF_6 at 35 °C, forming a yellow solution with no indication of $TcOF_5$ formation after 5 h. Upon separation, the components were examined by Raman spectroscopy; the volatile fraction was found to contain only XeF_6, and the involatile fraction was $[Xe_2F_{11}][TcO_2F_4]$ (eq 1).

Krypton difluoride is a sufficiently strong fluorinating agent to fluorinate TcO_2F_3 to $TcOF_5$ in anhydrous HF. A 10-fold molar excess of KrF_2 was initially used because of the competing decomposition of the KrF_2 to Kr and F_2 at room temperature over the 48 h period required for complete reaction (eq 2). The

$$TcO_2F_3 + KrF_2 \xrightarrow{HF} TcOF_5 + Kr + {}^1/_2O_2 \qquad (2)$$

unfavorable kinetics are thought to be the result of the strong Tc−O double bond and the insolubility of TcO_2F_3 in HF. The reaction was repeated using the HF-soluble $[Cs][TcO_2F_4]$ salt with the view that the negative charge would render the Tc−O bonds more polar and the oxygen more susceptible to electrophilic attack and oxidation by KrF^+ (eq 3); however, the reaction

$$[Cs][TcO_2F_4] + KrF_2 + xHF \xrightarrow{HF} TcOF_5 + Kr + {}^1/_2O_2 + [Cs][(HF)_xF] \qquad (3)$$

rate did not increase significantly. Periodic sonication of a mixture of TcO_2F_3 and a 5-fold molar excess of KrF_2 in HF at room temperature over a period of 24 h followed by removal of the solvent under vacuum at −78 °C proved to be the most efficient method for the preparation of $TcOF_5$. The resulting volatile orange solid melts reversibly and without decomposition at 57−58 °C and is deep red-orange in color in the liquid state. When maintained under anhydrous conditions, the solid is stable for at least two weeks at room temperature and is stable indefinitely when stored at −78 °C.

(b) Characterization of $TcOF_5$ by X-ray Crystallography. Details of the data collection parameters and other crystallographic information are given in Table 1 and the Supporting Information. Important bond lengths, bond valences, and bond angles are listed in Table 2. The closest intermolecular contacts are 2.941 (F(3)···O/F(1)) and 2.9537 (F(2)···F(3)) Å, which are significantly greater than the sums of the van der Waals radii (2.80 Å for F···F and 2.82 Å for F···O).

Technetium oxide pentafluoride crystallizes with the expected pseudooctahedral C_{4v} point symmetry. The structure, however, exhibits a 2-fold disorder with respect to a pseudo mirror plane. The mirror plane contains one of the F_e−Tc−F_e axes and bisects either pair of dihedral (90°) angles formed by the mutually perpendicular [O, F_e, F_e, F_a] and [F_e, F_e, F_e, F_e] planes so that, upon reflection through the pseudo mirror plane, the O atom and one of the F_e atoms interchange, the F_a atom and the remaining F_e atom interchange and two F_e atoms remain unshifted. The location of two nondisordered Tc−F_e bond lengths enabled the calculation of the Tc−O and Tc−F_a bond lengths (Figure 1 and Table 2).

The Tc−O bond length (1.67(1) Å) and Tc−F bond lengths are characteristic of a Tc^{VII}−O double bond and Tc^{VII}−F bond lengths.[6,8,13] The trans influence is clearly manifested in $TcOF_5$, where the *trans*-oxo Tc−F_a bond length (1.90(1) Å) is found to be significantly longer than the Tc−F_e bond length (1.81(1)

(15) Schrobilgen, G. J.; Holloway, J. H.; Russell, D. R. *J. Chem. Soc., Dalton Trans.* **1984**, 1411.
(16) Paine, R. T.; McDowell, R. S. *Inorg. Chem.* **1974**, *13*, 2366.
(17) Paine, R. T.; Treuil, K. L.; Stafford, F. E. *Spectrochim. Acta* **1973**, *29A*, 1891.
(18) LeBlond, N.; Schrobilgen, G. J. *J. Chem. Soc., Chem. Commun.* **1996**, 2479.

Table 2. Bond Lengths (Å), Bond Valences (vu), and Bond Angles (deg) in $TcOF_5$ and $[Tc_2O_2F_9][Sb_2F_{11}]$

$TcOF_5$

Bond Lengths (Å)

Tc(1)−O/F(2)	1.742(4)	Tc(1)−F(2)	1.822(9)	Tc(1)−F(3)	1.852(4)
Tc(1)−O/F(1)	1.740(10)	Tc(1)−F(1)	1.803(8)	Tc(1)−F(4)	1.859(7)

Calculated[a] Experimental Bond Lengths (Å) and Corresponding Bond Valences (vu)[b]

	Tc(1)−O	Tc(1)−F_e	Tc(1)−F_a
bond valence	1.812	1.056	0.828
bond length	1.67(1)	1.81(1)	1.90(1)

total bond valence 6.864

Bond Angles (deg)

O/F(2)−Tc(1)−O/F(1)	98.7(5)	O/F(2)−Tc(1)−F(2)	90.6(4)	O/F(1)−Tc(1)−F(2)	92.0(2)
O/F(2)−Tc(1)−F(1)	87.6(4)	O/F(1)−Tc(1)−F(1)	91.3(5)	F(2)−Tc(1)−F(1)	176.4(5)
O/F(2)−Tc(1)−F(4)	92.3(4)	O/F(1)−Tc(1)−F(4)	169.1(4)	F(2)−Tc(1)−F(4)	88.0(5)
F(1)−Tc(1)−F(4)	88.9(2)	O/F(2)−Tc(1)−F(3)	174.5(4)	O/F(1)−Tc(1)−F(3)	86.5(4)
F(2)−Tc(1)−F(3)	91.0(4)	F(1)−Tc(1)−F(3)	90.6(4)	F(4)−Tc(1)−F(3)	82.5(4)

$[Tc_2O_2F_9][Sb_2F_{11}]$

Bond Lengths (Å) and Corresponding Bond Valences (vu)[b]

	Tc(1)−O(1)	Tc(1)−F(1)	Tc(1)−F(2,2A)	Tc(1)−F(3)	Tc(1)−F(4)
bond valence	1.997	1.132	1.139	1.117	0.536
bond length[c]	1.634(6)	1.784(4)	1.782(4)	1.789(4)	2.061(3)
	[1.671]	[1.835]	[1.840, 1.842]	[1.835]	[2.091]

total bond valence 7.06

	Tc(2)−O(2)	Tc(2)−F(5)	Tc(2)−F(6,6A)	Tc(2)−F(7)	Tc(2)−F(4)
bond valence	2.025	1.087	1.117	1.114	0.516
bond length[c]	1.629(6)	1.799(4)	1.789(4)	1.790(4)	2.075(3)
	[1.671]	[1.834]	[1.839, 1.834]	[1.839]	[2.086]

total bond valence 6.98

	Sb(1)−F(8)	Sb(1)−F(9)	Sb(1)−F(10)	Sb(1)−F(11)	Sb(1)−F(12)	Sb(1)−F(13)
bond valence	0.883	0.910	0.869	0.881	0.885	0.544
bond length	1.843(3)	1.832(5)	1.849(3)	1.844(3)	1.842(3)	2.022(1)

total bond valence 4.97

Bond Angles in the $Tc_2O_2F_9^+$ Cation (deg)[c]

O(1)−Tc(1)−F(1)	97.7(2) [98.8]	F(6)−Tc(2)−F(6A)	163.7(2) [162.7]
O(1)−Tc(1)−F(2)	98.0(1) [99.2]	F(6)−Tc(2)−F(7)	89.2(1) [88.8]
O(1)−Tc(1)−F(3)	98.1(2) [98.8]	F(7)−Tc(2)−F(4)	81.7(2) [81.3]
O(1)−Tc(1)−F(4)	178.8(2) [179.7]	Tc(1)−F(4)−Tc(2)	158.2(2) [160.0]
F(1)−Tc(1)−F(2)	89.3(1) [88.9]	F(9)−Sb(1)−F(8)	95.6(1)
F(1)−Tc(1)−F(3)	164.2(2) [162.3]	F(9)−Sb(1)−F(10)	95.0(2)
F(1)−Tc(1)−F(4)	81.0(2) [81.2]	F(9)−Sb(1)−F(11)	95.2(2)
F(2)−Tc(1)−F(2A)	164.0(3) [162.1]	F(9)−Sb(1)−F(12)	95.6(2)
F(2)−Tc(1)−F(3)	88.5(1) [88.9]	F(9)−Sb(1)−F(13)	179.3(2)
F(2)−Tc(1)−F(4)	82.0(1) [81.12]	F(8)−Sb(1)−F(10)	169.4(2)
F(3)−Tc(1)−F(4)	83.1(2) [81.2]	F(8)−Sb(1)−F(11)	89.9(2)
O(2)−Tc(2)−F(4)	179.5(2) [179.7]	F(8)−Sb(1)−F(12)	89.4(2)
O(2)−Tc(2)−F(5)	98.4(2) [98.8]	F(8)−Sb(1)−F(13)	84.9(2)
O(2)−Tc(2)−F(6)	98.2(1) [98.8]	F(10)−Sb(1)−F(11)	89.0(2)
O(2)−Tc(2)−F(7)	97.8(2) [98.5]	F(10)−Sb(1)−F(12)	89.7(2)
F(5)−Tc(2)−F(4)	82.2(2) [81.4]	F(10)−Sb(1)−F(13)	84.5(2)
F(5)−Tc(2)−F(6)	88.5(1) [88.9]	F(11)−Sb(1)−F(12)	169.2(2)
F(5)−Tc(2)−F(7)	163.8(2) [162.7]	F(11)−Sb(1)−F(13)	85.3(2)
F(6)−Tc(2)−F(4)	81.4(1) [81.4]	Sb(1)−F(13)−Sb(1A)	172.8(3)

[a] The location of two nondisordered Tc−F_e bond lengths (1.81 Å) enabled the calculation of the Tc−O and Tc−F_a bond lengths: $Tc{-}O = 2 \times 1.741 - Tc{-}F_e$ and $Tc{-}F_a = 2 \times 1.856 - Tc{-}F_e$. [b] Bond valence units (vu) are defined in refs 41−43. $R_o = 1.89$ ($Tc^{VII}{=}O$), $R_o = 1.83$ ($Tc^{VII}{-}F$), and $R_o = 1.797$ ($Sb^{V}{-}F$) were used along with $B = 0.37$: Brown, I. D., Department of Physics, McMaster University, Hamilton, Ontario L8S 4M1, Canada, private communication. [c] Calculated values (LDFT/DZVP) for the $Tc_2O_2F_9^+$ cation are reported in square brackets.

Å), a trend already observed experimentally in $NbOF_5^{2-}$ [2.099(8) (F_a) and 1.932(7) (F_e) Å][19] and theoretically in $CrOF_5^-$ (Cr−F_a, 1.8318 Å; Cr−F_e, 1.7530 Å).[20] This trend has also been confirmed by LDFT calculations for $ReOF_5$ and $OsOF_5$ (see Computational Results *and* Normal Coordinate Analyses and Force Constants).

The compression of the F_e−Tc−F_e angles is readily apparent from the angle subtended by the nondisordered pair of equatorial

(19) Halasyamani, P.; Willis, M. J.; Stern, C. L.; Lundquist, P. M.; Wong, G. K.; Poeppelmeier, K. R. *Inorg. Chem.* **1996**, *35*, 1367.

(20) Gillespie, R. J.; Bytheway, I.; Tang, T. H.; Bader, R. F. *Inorg. Chem.* **1996**, *35*, 3954.

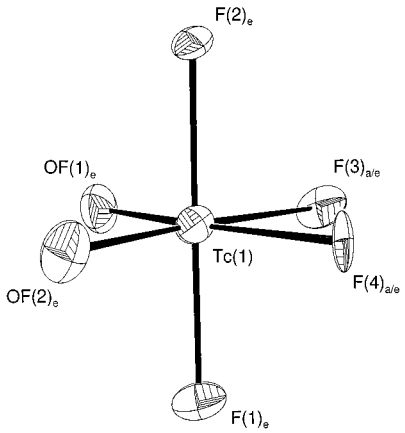

Figure 1. Structure of $TcOF_5$ showing the O/F_e and F_a/F_e disorder. Thermal ellipsoids are shown at the 50% probability level.

fluorines at technetium (176.4(5)°) and is attributable to the greater repulsion between the Tc−O and Tc−F_e bond pair domains than between the bond pair domains of Tc−O and Tc−F_a. Because of O/F_e and F_a/F_e disorder, the F_e−Tc−F_e angle compression away from Tc−O is expected to be significantly greater in the ordered structure and is verified by the calculated geometry (see the Computational Results).

The total bond valence at Tc is 6.86 vu (valence units) with contributions of 1.81 vu for the oxygen atom, 1.06 vu/equatorial fluorine atom, and 0.83 for the axial fluorine. The values for the Tc−O and Tc−F_e bonds are significantly less than their counterparts in the $Tc_2O_2F_9^+$ cation (Table 2), and are consistent with the anticipated greater bond polarities in the neutral species. The axial value shows that the Tc−F_a bond is significantly more ionic that the Tc−F_e bonds and similar in ionic character to the *trans*-oxo Tc−F bonds in $TcO_2F_4^-$ [7] but more covalent than the *trans*-fluoro Tc−F bonds of $TcO_2F_4^-$.

(c) NMR Spectroscopy. The gross solution structure of $TcOF_5$ was unambiguously established by ^{19}F NMR spectroscopy.[21] At −110 °C in SO_2ClF solvent, the $^{99}Tc-^{19}F$ couplings are quadrupole collapsed as a result of the long rotational correlation time of $TcOF_5$ at this temperature. The spectrum (Figure 2) consists of a doublet at 364.1 ppm and a quintet at 62.0 ppm having relative integrated intensities of 4.0:1.0, and which assigned to the equatorial (F_e) and the axial fluorines (F_a), respectively, consistent with the pseudooctahedral geometry found in the X-ray crystal structure of $TcOF_5$ (see X-ray Crystallography). The two-bond fluorine−fluorine coupling, $^2J(^{19}F_a-^{19}F_e) = 75$ Hz, is very similar in magnitude to that of $ReOF_5$ (69 Hz).[21] The ^{19}F resonances of $TcOF_5$ occur at 371.7 ppm (F_e, $\Delta\nu_{1/2} = 4930$ Hz) and 45.0 ppm (F_a, $\Delta\nu_{1/2} = 1840$ Hz), respectively, at 35 °C in HF solvent (Figure 2), but are broadened by partially quadrupole-collapsed spin−spin coupling to the ^{99}Tc nucleus. The ^{19}F spectrum at 31 °C in SO_2ClF shows two severely quadrupole broadened fluorine resonances at 373 ppm ($\Delta\nu_{1/2} = 9970$ Hz) for F_e and 60 ppm ($\Delta\nu_{1/2} = 6770$ Hz) for F_a. This behavior is consistent with the higher viscosity of SO_2ClF, which imparts a longer molecular correlation time to $TcOF_5$ and further decreases the short quadrupole-dominated T_1-relaxation time of ^{99}Tc. The effect is also manifested in the ^{99}Tc NMR spectrum (67.520 MHz) of $TcOF_5$ recorded at 31 °C in SO_2ClF, which shows a significantly broader resonance (433.8 ppm, $\Delta\nu_{1/2} = 6705$ Hz) than that recorded at 25 °C in SO_2ClF (394.5, $\Delta\nu_{1/2} = 438$ Hz). Consequently, no $^1J(^{99}Tc-^{19}F)$ couplings could be resolved in either the ^{19}F or ^{99}Tc NMR spectra because of quadrupolar broadening resulting from the fast relaxation rate of the ^{99}Tc nucleus. The ^{19}F line widths are consistent with a larger $^1J(^{99}Tc-^{19}F_e)$ coupling than for $^1J(^{99}Tc-^{19}F_a)$ coupling. The ^{19}F resonance of the equatorial fluorines of $TcOF_5$ and the ^{99}Tc resonance are significantly more deshielded than TcO_3F,[5] TcO_3^+,[5] $TcO_2F_4^-$,[7] and $TcO_2F_3(CH_3CN)$.[7] As observed for $ReOF_5$,[21] the shielding of the axial fluorine is substantially greater relative to that of the equatorial fluorines in $TcOF_5$ ($\Delta\delta(^{19}F) = 326.7$ ppm (SO_2ClF), 302.1 ppm (HF)). Both the relative ^{19}F line widths and ^{19}F chemical shifts are consistent with a significantly more ionic Tc−F_a bond, which is in accord with the longer Tc−F_a bond length observed in the X-ray structure and the trans influence of the Tc−O double bond.

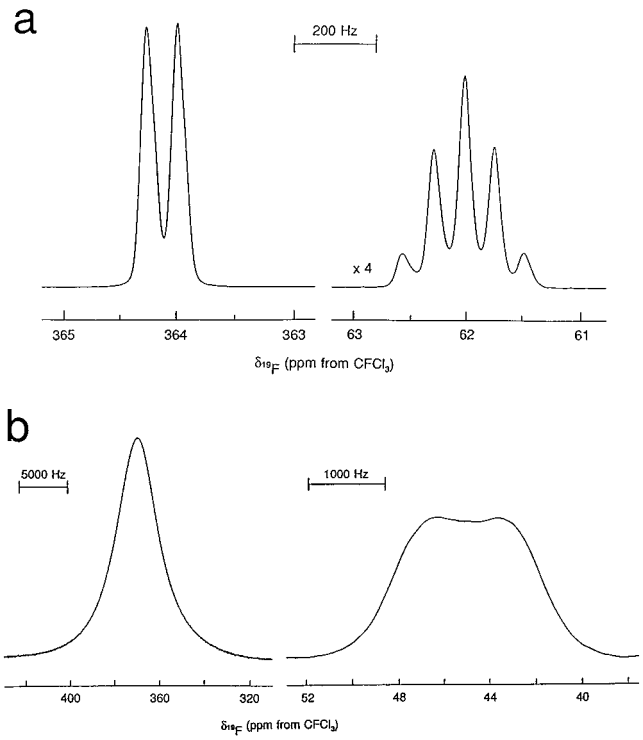

Figure 2. ^{19}F NMR spectra (282.409 MHz) of (a) $TcOF_5$ dissolved in SO_2ClF solvent at −110 °C and (b) $TcOF_5$ dissolved in HF at 30 °C.

The reaction between ^{17}O-enriched TcO_4^- and excess KrF_2 in HF was previously investigated, but the product was mistakenly assigned to TcO_2F_3.[5] It is now apparent that the product observed by solution NMR was $TcOF_5$, cf $\delta(^{99}Tc) = 396.3$ ppm (25 °C, $\Delta\nu_{1/2} = 375$ Hz), $\delta(^{17}O) = 1211$ ppm (25 °C, $\Delta\nu_{1/2} = 700$ Hz), and $\delta(^{19}F_a) = -6.5$ ppm (−47 °C, $\Delta\nu_{1/2} = 370$ Hz); $\delta(^{19}F_e)$ was not observed.

(d) Vibrational Spectroscopy. The Raman spectra of $TcOF_5$ in the solid state (22 and −150 °C) and in HF solution (22 °C) are shown in Figure 3, and the infrared spectrum is shown in Figure 4. The observed frequencies and their assignments are listed in Table 3. The 15 vibrational modes of $TcOF_5$ under C_{4v} point symmetry belong to the irreducible representations $4A_1 + 2B_1 + B_2 + 4E$, which are all Raman active, and the A_1 and E modes, which are infrared active. Although the Raman spectra of the solid recorded at 22 and −150 °C are similar, they differ in that the bands in the low-temperature spectrum are extensively split and, in addition, two new bands appear at 217 and 716 cm^{-1}. The spectral differences suggest that $TcOF_5$ exists as two phases and extensive vibrational coupling within the unit cell of the low-temperature phase is responsible for the additional splittings and the new bands. Using the unit cell from

(21) Bartlett, N.; Beaton, S.; Reeves, L. W.; Wells, E. J. *Can. J. Chem.* **1964**, *42*, 2531.

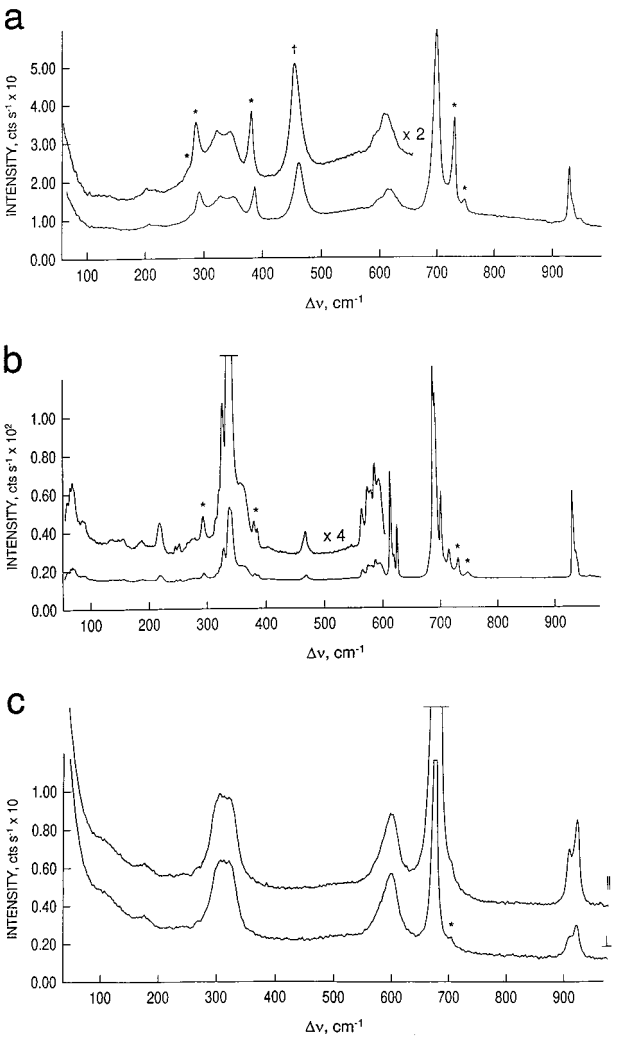

Figure 3. Raman spectra of microcrystalline $TcOF_5$ recorded using 647.1 nm excitation at (a) 22 °C and (b) −150 °C and of (c) an HF solution of $TcOF_5$ at 22 °C, with the analyzer oriented parallel (∥) and perpendicular (⊥) to the polarization of the incident beam. Asterisks denote FEP sample tube lines, and the dagger denotes residual KrF_2.

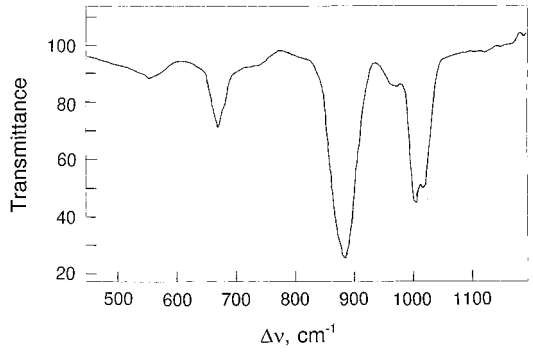

Figure 4. Gas-phase infrared spectrum of $TcOF_5$ recorded at 22 °C and ca. 1−2 Torr using a 10 cm FEP cell and AgCl windows.

the −102 °C structure of $TcOF_5$, a factor-group analysis (Supporting Information) was performed in which the free molecule symmetry (C_{4v}) was correlated to the crystal site symmetry (C_1) and to the unit cell symmetry (C_{2v}), predicting that each Raman-active vibrational band of $TcOF_5$ is split into three Raman- and infrared-active components, $A_1 + B_1 + B_2$.

The Raman and infrared spectra of $TcOF_5$ were assigned by analogy with the spectra of $ReOF_5$ and $OsOF_5$,[22] to which they are remarkably similar, and by comparison with the frequencies from LDFT calculations. The assignments were also aided by Raman polarization measurements on an HF solution of $TcOF_5$. The asymmetric TcF_{4e} stretching mode, $\nu_8(E)$, could not be observed in the Raman spectrum, which is consistent with the Raman spectra of $ReOF_5$ and $OsOF_5$, where this mode is also too weak to be observed.[22] The mode was, however, observed at 729 cm^{-1} in the gas-phase infrared spectrum. Although formally allowed in the Raman and infrared spectra, $\nu_{10}(E)$ is too weak to be observed in the Raman spectrum of an HF solution and in the Raman spectrum of the solid at 22 °C. Both $\nu_8(E)$ and $\nu_{10}(E)$ are rendered active in the low-temperature Raman spectrum of the solid and are assigned to factor-group components of $\nu_8(E)$ and $\nu_{10}(E)$ at 716 and 217 cm^{-1}, respectively. The 716 cm^{-1} Raman band occurs in the gas-phase infrared spectrum at 729 cm^{-1}, and the assignments of both E modes were confirmed by LDFT calculations (see Normal Coordinate Analyses *and* Computational Results). From their potential energy distributions (Table 4), $\nu_2(A_1)$ and $\nu_3(A_1)$ result from significant coupling between the MF_{4e} and MF_{ax} stretching modes. The degree of coupling between the analogous modes is greatest in $TeOF_5^-$,[23] comparable in $TcOF_5$, $OsOF_5$, and IOF_5,[24] and the least in $ReOF_5$. The bending modes $\nu_9(E)$, $\nu_{10}(E)$, and $\nu_{11}(E)$ are coupled to a significant extent and are comparable over the MOF_5 series, but are most strongly coupled in IOF_5 and $TeOF_5^-$.

Normal Coordinate Analyses and Force Constants. The Trans Influence in MOF_5 (M = Tc, Re, Os). The experimental structures of $TcOF_5$ (see the X-ray Crystal Structure of $TcOF_5$) and $NbOF_5^{2-}$ [19] and those calculated for $TcOF_5$, $ReOF_5$, and $OsOF_5$ in this work and for $CrOF_5^-$ [20] all manifest the trans influence[25,26] of oxygen by displaying $M-F_a$ bonds that are significantly longer than their $M-F_e$ bonds. The observed geometries of $TcOF_5$ and $NbOF_5^{2-}$ and those calculated for $ReOF_5$ and $OsOF_5$ also conform to the classical VSEPR (valence shell electron repulsion)[27] AX_4YZ geometry in that their ligand arrangements are pseudooctahedral and the four equatorial fluorines are bent away from the oxygen, consistent with the M−O bonds having multiple bond character. The lengthening of the M−F bond trans to an oxo ligand was more recently rationalized by Gillespie et al.[20] who performed SCF calculations on a number of chromium(VI) oxofluorides and studied the topologies of their electron densities and their Laplacians. The geometries adopted by these complexes, some of which do not agree with the predictions of the VSEPR model, were accounted for in terms of metal core electron distortions. The geometrical parameters of the $CrOF_5^-$ anion, which is isovalent with $TcOF_5$ and $ReOF_5$, were calculated and also exhibit a $Cr-F_a$ bond (1.8318 Å) that is significantly longer than the $Cr-F_e$ bonds (1.7530 Å) and $O-Cr-F_e$ angles (94.7°) that are opened up as in the corresponding angles calculated for $TcOF_5$ (94.3°), $ReOF_5$ (94.6°), and $OsOF_5$ (95.0°).

A previous report in which the normal coordinate analyses of $ReOF_5$ and $OsOF_5$ [9] were performed concluded that the axial $M-F_a$ bonds of both oxide pentafluorides are significantly more covalent than the $M-F_e$ bonds. The approach used seriously underdetermined the problem, leading to an infinite number of

(22) Holloway, J. H.; Selig, H.; Claassen, H. H. *J. Chem. Phys.* **1971**, *54*, 4305.
(23) Christe, K. O.; Dixon, D. A.; Sanders, J. C. P.; Schrobilgen, G. J.; Wilson, W. W. *Inorg. Chem.* **1993**, *32*, 4089.
(24) Christe, K. O.; Curtis, E. C.; Dixon, D. A. *J. Am. Chem. Soc.* **1993**, *115*, 9655.
(25) Chatt, J.; Duncanson, L. A.; Venanzi, L. M. *J. Chem. Soc.* **1955**, 4456.
(26) Orgel, L. E. *J. Inorg. Nucl. Chem.* **1956**, *2*, 137.
(27) Gillespie, R. J.; Hargittai, I. *The VSEPR Model of Molecular Geometry*; Allyn and Bacon: Boston, MA, 1991.

Table 3. Experimental and Calculated Raman Frequencies, Assignments, and Mode Descriptions for $TcOF_5$ in the Solid State and in HF Solution

frequencies (cm^{-1})						
exp[a]				LDFT[d]		assignments[e] (C_{4v} point symmetry)
solid (22 °C)[b]	solid (−150 °C)[b]	solution[b]	gas[c]	TZ94P	DZVP	
			1045			$\nu_8 + \nu_9$, combination band
952 (2)						$\nu_3 + \nu_4$, combination band
940 (14)	939 (14), sh	937 (4), p	930 (m)	988 (107)	972 (122)	$\nu_1(A_1)$, ν(TcO)
933 (28)	933 (45)					
			860 (w)			$\nu_5 + \nu_6$, combination band
	716 (16)		729 (s), sh	724 (388)	709 (400)	$\nu_8(E)$, $\nu_{as}(TcF_{4e})$
702 (100)	703 (47)	702 (100), p	716 (vs)	694 (37)	679 (38)	$\nu_2(A_1)$, $\nu_{sym}(TcF_a + TcF_{4e})$
	694 (95), sh					
	690 (100)					
616 (8)	626 (29)	624 (8), dp	631 (w)	627 (0)	612 (0)	$\nu_5(B_1)$, $\nu_{as}(TcF_{2e} - TcF_{2e})$
	620 (13), sh					
	614 (57)					
601 (5)	595 (9)	598 (2), sh, dp	596 (s)	623 (40)	608 (34)	$\nu_3(A_1)$, $\nu_{sym}(TcF_a - TcF_{4e})$
	588 (11)		582 (s)			
	581 (8)					
	575 (8)					
	565 (6)					
351 (10)	358 (8)	346 (10), dp		329 (4)	322 (4)	$\nu_9(E)$, $\delta_{as}(OTcF_e)$ scissors
328 (10)	337 (39)	329 (10), dp		315 (11)	299 (11)	$\nu_4(A_1)$, $\delta_{sym}(TcF_{4e})$, umbrella
	327 (18)					
	320 (8), sh					
	314 (3), sh					
278 (5)	293 (5)	289 (2), dp		278 (0)	286 (0)	$\nu_7(B_2)$, $\delta_{as}(TcF_{4e})$, scissors
	217 (3)			233 (60)	245 (60)	$\nu_{10}(E)$, $\delta_{as}(OTcF_a + TcF_{2e})$
207 (2)	186 (2)	199 (2), dp		207 (0)	191 (0)	$\nu_6(B_1)$, $\delta_{as}(TcF_{4e})$, out-of-plane pucker
131 (1)	154 (2)	135 (1), br, dp		63 (1)	97 (2)	$\nu_{11}(E)$, $\delta_{as}(OTcF_a - TcF_{2e})$
	139 (2)					
	84 (4)					
	66 (9)					

[a] Values in parentheses denote relative Raman intensities, and symbols denote shoulder (sh), broad (br), polarized (p), and depolarized (dp). [b] Spectra recorded in FEP using 647.1 nm excitation. [c] Infrared intensities are denoted as very strong (vs), strong (s), medium (m), or weak (w). [d] Calculated values using the theoretical geometrical parameters reported in Table 6; values in parentheses denote calculated infrared intensities, km mol^{-1}. [e] Symbols denote stretch (ν) and bend (δ).

solutions which duplicate a given frequency set and conclusions which contradict the experimental structures of $NbOF_5^{2-}$ [19] and $TcOF_5$ (see the X-ray Crystal Structure of $TcOF_5$) and the calculated structures of $CrOF_5^-$,[20] $TcOF_5$, $ReOF_5$, and $OsOF_5$ (see the Computational Results). The problem has been overcome in the present study by using ab initio methods to arrive at a fully determined force field with off-diagonal symmetry force constants that are expected to be very close to those of the general valence force field on the basis of the good agreement between the calculated and experimental frequencies.

The force fields for the MOF_5 species have been calculated (Table 4) using the DZVP basis set for all atoms of $TcOF_5$ and for O and F in $ReOF_5$ and $OsOF_5$. For the latter two compounds, the Hay−Wadt ECP's were used for the Re and Os compounds. No scaling was applied to either the calculated frequencies or force fields. By using the symmetry-adapted internal coordinates from Smith and Begun[28] as used by Christe et al.,[23,24,29] we can convert our force constants, derived from the frequencies listed in Table 4, into internal force constants as shown in footnote *f* of Table 4. Our results show that the internal stretching force constants of the M−O bonds are in accord with their double bond characters as they are almost double the internal M−F stretching force constants. The internal $M-F_e$ stretching force constants are significantly greater than the $M-F_a$ ones, consistent with the lower $M-F_a$ bond order anticipated as a result of the trans influence of oxygen and with the relative bond lengths and bond orders in these molecules (see the X-ray Crystal Structure of $TcOF_5$ *and* Computational Results). This contrasts with the only known neutral main-group oxide pentafluoride, IOF_5, where the $I-F_e$ and $I-F_a$ bond lengths and their stretching force constants are found to be essentially equal.[24] The unimportance of the trans influence of the oxo ligand in IOF_5 may be ascribed to a lack of I−O $d\pi-p\pi$ bonding.

The vibrational frequencies of $TcOF_5$ are generally lower than their $ReOF_5$ and $OsOF_5$ counterparts. The trend is opposite that expected on the basis of reduced mass effect alone even though the metal undergoes displacement in all normal coordinates except $\nu_3(A_1)$, $\nu_5(B_1)$, and $\nu_7(B_2)$. The trend is consistent with our findings and with Tc−F and Tc−O bond stretching force constants which are lower than those of $ReOF_5$ and $OsOF_5$. The stretching force constants involving the axial ligands of $OsOF_5$ are predicted to be slightly higher than those in $ReOF_5$, whereas the reverse is true for the $M-F_e$ force constants. Decreases in $\nu_1(A_1)$ with decreasing mass within a group have also been noted for TcF_6/ReF_6, TcF_6^-/ReF_6^-, MoF_6/WF_6, MoF_6^-/WF_6^-, IrF_6/OsF_6, and IrF_6^-/OsF_6^-.[30]

Fluoride-Ion Donor Properties of $TcOF_5$. (a) Synthesis of the $Tc_2O_2F_9^+$ Cation and the Attempted Synthesis of TcF_6^+. When HF solutions of $TcOF_5$ are allowed to react with 5-fold molar excesses of the strong Lewis acid AsF_5 or SbF_5, bright yellow precipitates are formed. After removal of the solvent and excess Lewis acid, both solids are stable at room temperature for at least 3 days under dry nitrogen. The reaction between

(28) Smith, D. F.; Begun, G. M. *J. Chem. Phys.* **1965**, *43*, 2001.
(29) Christe, K. O.; Schack, C. J.; Pilipovich, D.; Curtis, E. C.; Sawodny, W. *Inorg. Chem.* **1973**, *12*, 620.
(30) Shamir, J.; Malm, J. G. *J. Inorg. Nucl. Chem. Suppl.* **1976**, 107.

Table 4. Ab Initio Force Fields and Potential Energy Distributions of MOF_5 (M = Tc, Re, Os)

point group C_{4v}	assignment	calcd freq, cm^{-1} [a]	symmetry force constants[b–f]	PED (%)[c]
			$TcOF_5$	
A_1	ν_1	972 (122)	$F_{1,1} = f_D = 7.65$ $F_{1,2} = f_{DR} = 0.35$ $F_{1,3} = f_{Dr} = 0.27$ $F_{1,4} = -0.09$	92.0 (S_1) + 3.1 (S_3) + 4.9 (S_4)
	ν_2	679 (38)	$F_{2,2} = f_R = 4.73$ $F_{2,3} = f_{Rr} = 0.32$ $F_{2,4} = -0.16$	57.3 (S_2) + 39.3 (S_3) + 3.4 (S_4) (symmetric combination of S_2 and S_3)
	ν_3	608 (34)	$F_{3,3} = f_r + 2f_{rr} + f_{rr'} = 3.94$ $F_{3,4} = 0.27$	33.2 (S_2) + 65.3 (S_3) + 1.0 (S_4) (antisymmetric combination of S_2 and S_3)
	ν_4	299 (11)	$F_{4,4} = {}^1/_2(f_\beta + 2f_{\beta\beta} + f_{\beta\beta'} + f_\gamma + 2f_{\gamma\gamma} + f_{\gamma\gamma'} - 2f_{\beta\gamma} - 4f_{\beta\gamma'} - 2f_{\beta\gamma''}) = 1.12$	99.6 (S_4)
B_1	ν_5	612 (0)	$F_{5,5} = f_r - 2f_{rr} + f_{rr'} = 4.19$ $F_{5,6} = -0.19$	99.9 (S_5)
	ν_6	191 (0)	$F_{6,6} = {}^1/_2(f_\beta - 2f_{\beta\beta} + f_{\beta\beta'} + f_\gamma - 2f_{\gamma\gamma} + f_{\gamma\gamma'} - 2f_{\beta\gamma} + 4f_{\beta\gamma'} - 2f_{\beta\gamma''}) = 0.71$	99.7 (S_6)
B_2	ν_7	286 (0)	$F_{7,7} = f_\alpha - 2f_{\alpha\alpha} + f_{\alpha\alpha'} = 0.80$	100 (S_7)
E	ν_8	709 (400)	$F_{8,8} = f_r - f_{rr'} = 4.24$ $F_{8,9} = f_{r\beta} - f_{r\beta''} = 0.33$ $F_{8,10} = f_{r\gamma} - f_{r\gamma'} = 0.19$ $F_{8,11} = \sqrt{2}(f_{r\alpha} - f_{r\alpha'}) = -0.21$	93.6 (S_8) + 1.4 (S_9) + 1.4 (S_{10}) + 3.5 (S_{11})
	ν_9	322 (4)	$F_{9,9} = f_\beta - f_{\beta\beta'} = 0.64$ $F_{9,10} = -0.26$ $F_{9,11} = -0.20$	67.0 (S_9) + 31.9 (S_{10})
	ν_{10}	245 (60)	$F_{10,10} = f_\gamma - f_{\gamma\gamma'} = 0.66$ $F_{10,11} = -0.18$	16.9 (S_9) + 31.7 (S_{10}) + 51.1 (S_{11})
	ν_{11}	97 (2)	$F_{11,11} = f_\alpha - f_{\alpha\alpha'} = 0.80$	30.5 (S_9) + 30.0 (S_{10}) + 39.4 (S_{11})
			$ReOF_5$	
A_1	ν_1	1010 (101)	$F_{1,1} = f_D = 8.87$ $F_{1,2} = f_{DR} = 0.37$ $F_{1,3} = f_{Dr} = 0.40$ $F_{1,4} = -0.03$	98.0 (S_1) + 1.5 (S_4)
	ν_2	716 (29)	$F_{2,2} = f_R = 5.50$ $F_{2,3} = f_{Rr} = 0.38$ $F_{2,4} = -0.16$	79.2 (S_2) + 19.4 (S_3) + 1.0 (S_4) (symmetric combination of S_2 and S_3)
	ν_3	633 (62)	$F_{3,3} = f_r + 2f_{rr} + f_{rr'} = 4.35$ $F_{3,4} = 0.27$	15.9 (S_2) + 83.5 (S_3) (antisymmetric combination of S_2 and S_3)
	ν_4	293 (15)	$F_{4,4} = {}^1/_2(f_\beta + 2f_{\beta\beta} + f_{\beta\beta'} + f_\gamma + 2f_{\gamma\gamma} + f_{\gamma\gamma'} - 2f_{\beta\gamma} - 4f_{\beta\gamma'} - 2f_{\beta\gamma''}) = 1.23$	99.7 (S_4)
B_1	ν_5	654 (0)	$F_{5,5} = f_r - 2f_{rr} + f_{rr'} = 4.79$ $F_{5,6} = -0.18$	99.9 (S_5)
	ν_6	206 (0)	$F_{6,6} = {}^1/_2(f_\beta - 2f_{\beta\beta} + f_{\beta\beta'} + f_\gamma - 2f_{\gamma\gamma} + f_{\gamma\gamma'} - 2f_{\beta\gamma} + 4f_{\beta\gamma'} - 2f_{\beta\gamma''}) = 0.82$	99.8 (S_6)
B_2	ν_7	300 (0)	$F_{7,7} = f_\alpha - 2f_{\alpha\alpha} + f_{\alpha\alpha'} = 0.86$	100 (S_7)
E	ν_8	710 (180)	$F_{8,8} = f_r - f_{rr'} = 4.79$ $F_{8,9} = f_{r\beta} - f_{r\beta''} = 0.29$ $F_{8,10} = f_{r\gamma} - f_{r\gamma'} = 0.17$ $F_{8,11} = \sqrt{2}(f_{r\alpha} - f_{r\alpha'}) = -0.20$	97.9 (S_8) + 1.2 (S_{11})
	ν_9	340 (2)	$F_{9,9} = f_\beta - f_{\beta\beta'} = 0.75$ $F_{9,10} = -0.27$ $F_{9,11} = -0.19$	66.6 (S_9) + 33.1 (S_{10})
	ν_{10}	238 (33)	$F_{10,10} = f_\gamma - f_{\gamma\gamma'} = 0.72$ $F_{10,11} = -0.20$	19.5 (S_9) + 32.6 (S_{10}) + 47.6 (S_{11})
	ν_{11}	110 (0)	$F_{11,11} = f_\alpha - f_{\alpha\alpha'} = 0.53$	24.6 (S_9) + 29.2 (S_{10}) + 46.1 (S_{11})
			$OsOF_5$	
A_1	ν_1	1013 (82)	$F_{1,1} = f_D = 8.94$ $F_{1,2} = f_{DR} = 0.33$ $F_{1,3} = f_{Dr} = 0.25$ $F_{1,4} = -0.08$	97.9 (S_1) + 1.4 (S_4)
	ν_2	698 (35)	$F_{2,2} = f_R = 5.06$ $F_{2,3} = f_{Rr} = 0.37$ $F_{2,4} = -0.16$	59.9 (S_2) + 38.9 (S_3) + 1.1 (S_4) (symmetric combination of S_2 and S_3)
	ν_3	631 (33)	$F_{3,3} = f_r + 2f_{rr} + f_{rr'} = 4.47$ $F_{3,4} = 0.32$	34.9 (S_2) + 64.9 (S_3) (antisymmetric combination of S_2 and S_3)
	ν_4	277 (17)	$F_{4,4} = {}^1/_2(f_\beta + 2f_{\beta\beta} + f_{\beta\beta'} + f_\gamma + 2f_{\gamma\gamma} + f_{\gamma\gamma'} - 2f_{\beta\gamma} - 4f_{\beta\gamma'} - 2f_{\beta\gamma''}) = 1.14$	99.5 (S_4)

Table 4 (Continued)

point group C_{4v}	assignment	calcd freq, cm^{-1} [a]	symmetry force constants[b–f]	PED (%)[c]
			$OsOF_5$	
B_1	ν_5	641 (0)	$F_{5,5} = f_r - 2f_{rr} + f_{rr'} = 4.59$ $F_{5,6} = -0.20$	99.9 (S_5)
	ν_6	201 (0)	$F_{6,6} = {}^1/_2(f_\beta - 2f_{\beta\beta} + f_{\beta\beta'} + f_\gamma - 2f_{\gamma\gamma} + f_{\gamma\gamma'} - 2f_{\beta\gamma} + 4f_{\beta\gamma'} - 2f_{\beta\gamma''}) = 0.80$	99.8 (S_6)
B_2	ν_7	229 (0)	$F_{7,7} = f_\alpha - 2f_{\alpha\alpha} + f_{\alpha\alpha'} = 0.51$	100 (S_7)
E	ν_8	701 (146)	$F_{8,8} = f_r - f_{rr'} = 4.65$ $F_{8,9} = f_{r\beta} - f_{r\beta''} = 0.31$ $F_{8,10} = f_{r\gamma} - f_{r\gamma'} = 0.20$ $F_{8,11} = \sqrt{2}(f_{r\alpha} - f_{r\alpha'}) = -0.02$	97.5 (S_8) + 1.7 (S_{11})
	ν_9	329 (1)	$F_{9,9} = f_\beta - f_{\beta\beta'} = 0.70$ $F_{9,10} = -0.20$ $F_{9,11} = -0.22$	61.6 (S_9) + 38.1 (S_{10})
	ν_{10}	264 (21)	$F_{10,10} = f_\gamma - f_{\gamma\gamma'} = 0.85$ $F_{10,11} = -0.15$	17.5 (S_9) + 28.3 (S_{10}) + 54.1 (S_{11})
	ν_{11}	147 (2)	$F_{11,11} = f_\alpha - f_{\alpha\alpha'} = 0.81$	39.3 (S_9) + 26.7 (S_{10}) + 33.7 (S_{11})

[a] Calculated values using the theoretical geometrical parameters reported in Table 6; values in parentheses denote calculated infrared intensities, in km mol^{-1}. [b] Stretching constants, mdyn $Å^{-1}$; deformation constants, mdyn Å rad^{-2}; stretch–bend interaction constants, mdyn rad^{-1}. [c] The following symmetry coordinates were used and appear in the potential energy distribution (PED): S_1 = MO stretch; S_2 = MF_a stretch; S_3 = MF_4 sym in-phase stretch; S_4 = MF_4 umbrella deformation; S_5 = MF_4 sym out-of-phase stretch; S_6 = MF_6 pucker deformation; S_7 = MF_4 sym in-plane deformation; S_8 = MF_4 asym stretch; S_9 = MF_a wag; S_{10} = MO wag; S_{11} = MF_4 asym in-plane deformation. Their explicit forms are given in ref 23, 24, 28, 29. [d] The missing explicit *F*-matrix terms are complex, angle-dependent expressions and, therefore, are not listed. [e] The following internal coordinates were used: M–O = D, M–F_a = R, M–F_e = r, $\angle F_e$–M–$F_e = \alpha$, $\angle F_e$–M–O = γ, $\angle F_e$–M–$F_a = \beta$. [f] Internal force constants: $TcOF_5$, f_D = 7.65; f_R = 3.94, f_r = 4.35; $ReOF_5$, f_D = 8.87; f_R = 4.35, f_r = 4.97; $OsOF_5$; f_D = 8.94; f_R = 4.47, f_r = 4.74.

$TcOF_5$ and SbF_5 was shown (see the X-ray Crystal Structure of $[Tc_2O_2F_9][Sb_2F_{11}]$) to proceed according to eq 4, and is

$$2TcOF_5 + 2SbF_5 \xrightarrow{HF} [Tc_2O_2F_9][Sb_2F_{11}] \qquad (4)$$

analogous to the $ReOF_5/SbF_5$[15] and OsO_2F_4/SbF_5[11] systems which yield the binuclear $Re_2O_2F_9^+$ and $Os_2O_4F_7^+$ cations, respectively. The AsF_6^- salt resulted from an attempt to synthesize the TcF_6^+ cation (vide infra).

The synthesis of the TcF_6^+ cation is of particular interest because it is a precursor to the unknown heptafluoride, TcF_7. The ReF_6^+ cation has been previously synthesized by the interaction of ReF_7 with strong fluoride ion acceptors and structurally characterized.[15,31] Previous attempts to prepare TcF_6^+ salts by oxidative fluorination of TcF_6 with KrF^+ salts were unsuccessful.[32] In our most recent attempt to prepare TcF_6^+, $TcOF_5$ was allowed to react with a 5-fold molar excess of [KrF][AsF_6] in HF in an attempt to prepare [TcF_6][AsF_6] according to eq 5. No evidence for TcF_6^+ was found by Raman

$$2TcOF_5 + 3[KrF][AsF_6] \xrightarrow[0\ °C]{HF} 2[TcF_6][AsF_6] + 3Kr + [O_2][AsF_6] + {}^1/_2\ F_2 \qquad (5)$$

spectroscopy, nor was the O–O stretching mode corresponding to the formation of [O_2][AsF_6] observed in the Raman spectrum (1858 cm^{-1}).[33] Instead, a bright yellow solid precipitated from solution that was identified by Raman spectroscopy as [$Tc_2O_2F_9$]-[AsF_6] (eq 6). This behavior is similar to that observed in the

$$2TcOF_5 + [KrF][AsF_6] \xrightarrow{HF} [Tc_2O_2F_9][AsF_6] + Kr + {}^1/_2\ F_2 \qquad (6)$$

reaction of OsO_2F_4 with [KrF][AsF_6], which did not result in further fluorination to give the $OsOF_5^+$ cation, but only resulted in the formation of $Os_2O_4F_7^+$.[11] In both reactions, [KrF][AsF_6] decomposes at a moderate rate at room temperature to Kr, F_2, and AsF_5. The AsF_5 liberated in the decomposition of [KrF]-[AsF_6] is expected to form metal oxide fluoride cations such as $TcOF_4^+$ and $Tc_2O_2F_9^+$ (vide infra), which, because of their greater electron deficiencies, are more difficult to oxidize and which also pose kinetic (Coulombic) barriers to oxidative fluorination by another cationic oxidizer. Consequently, the reaction between $TcOF_5$ and AsF_5 proceeds according to eq 7,

$$2TcOF_5 + AsF_5 \xrightarrow{HF} [Tc_2O_2F_9][AsF_6] \qquad (7)$$

by analogy with the $OsO_2F_4/KrF^+AsF_6^-$ system.[11] The bands attributed to the cation in the Raman spectrum of [$Tc_2O_2F_9$]-[AsF_6] are nearly identical in frequency and relative intensity to those of [$Tc_2O_2F_9$][Sb_2F_{11}], and the remaining anion bands are assigned to octahedral AsF_6^- with no bands attributable to the $As_2F_{11}^-$ anion[34] (see Raman Spectroscopy).

(b) X-ray Crystal Structure of [$Tc_2O_2F_9$][Sb_2F_{11}]. Details of the data collection parameters, the unit cell, and other crystallographic information are given in Table 1 and in the Supporting Information. Important bond lengths, corresponding bond valences, and bond angles are listed in Table 2.

The structure of [$Tc_2O_2F_9$][Sb_2F_{11}] consists of well-separated $Tc_2O_2F_9^+$ cations and $Sb_2F_{11}^-$ anions (Figure 5). The closest cation–anion contact between an oxygen and a terminal fluorine ligand is 2.664(5) Å and is somewhat less than the sum of the van der Waals radii (2.82 Å),[35] whereas the closest interionic fluorine–fluorine contact is 2.894(4) Å, which is somewhat greater than the sum of the van der Waals radii (2.80 Å).[35] The cations are oriented parallel to the *b* axis of the unit cell (Supporting Information) and consist of two square pyramidal $TcOF_4$ units that are bridged by a fluorine and in which the oxygens are trans to the bridging fluorine. The structure of the cation is very similar to those of the valence-isoelectronic

(31) Bartlett, N.; Kourtakis, K.; Mallouk, T.; Yeh, S. *J. Fluorine Chem.* **1984**, *26*, 97.
(32) Schrobilgen, G. J.; Holloway, J. H. Unpublished results.
(33) Shamir, J.; Binenboym, J.; Claasen, H. H. *J. Am. Chem. Soc.* **1968**, *90*, 6223.
(34) Barraclough, C. G.; Besida, J.; Davies, P. G.; O'Donnell, T. A. *J. Fluorine Chem.* **1988**, *38*, 405.
(35) Bondi, A. *J. Phys. Chem.* **1964**, *68*, 441.

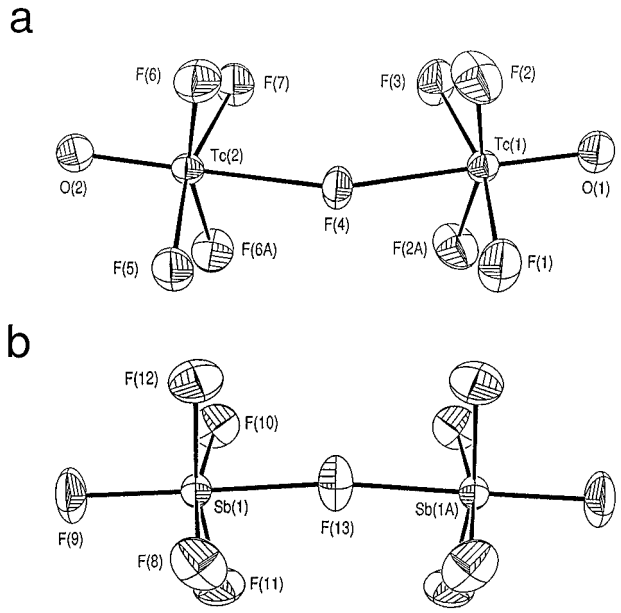

Figure 5. Structures of (a) the $Tc_2O_2F_9^+$ cation and (b) the $Sb_2F_{11}^-$ anion in $[Tc_2O_2F_9][Sb_2F_{11}]$ with thermal ellipsoids shown at the 50% probability level.

species $W_2O_2F_9^-$ [36] and $Re_2O_2F_9^+$ [15] as well as to $Mo_2O_2F_9^{3-}$ [37] and $V_2O_2F_8(H_2O)^{2-}$.[38] The $Sb_2F_{11}^-$ anions in $[Tc_2O_2F_9][Sb_2F_{11}]$ are oriented parallel to the *c* axis of the unit cell. The Sb−F_t and Sb−F_b bond lengths and bond angles in the $Sb_2F_{11}^-$ anion are similar to those reported previously, and the anion adopts an eclipsed conformation.[39,40]

As anticipated, the Tc−O bonds of the $Tc_2O_2F_9^+$ cation are less polar than that in $TcOF_5$, with Tc−O bond lengths (1.634(6) and 1.629(6) Å) that are slightly shorter than that of $TcOF_5$ (1.67(1) Å), but comparable to those found in the ionic $TcO_2F_3{\cdot}SbF_5$ adduct (1.640(6) and 1.643(5) Å).[8] The terminal Tc−F_t bond lengths (range 1.782(4)−1.799(4) Å) are also somewhat shorter and less polar than the Tc−F_e bonds in $TcOF_5$ (1.81(1) Å), but comparable to the Tc−F_t bonds in the $TcO_2F_3{\cdot}SbF_5$ adduct (1.800(5) and 1.804(5) Å). As expected, the bridging Tc−F_b bond lengths (2.061(3) and 2.075(3) Å) are considerably longer than the Tc−F_a bonds in $TcOF_5$ (1.90(1) Å), comparable to those in polymeric TcO_2F_3 (range 2.062(1)−2.106(6) Å),[6] but considerably shorter than the Tc−F_b bond lengths found in $TcO_2F_3{\cdot}SbF_5$ (2.217(4) and 2.222(4) Å). The trends parallel those observed among $ReOF_5$ (see the Computational Results), $Re_2O_2F_9^+$,[15] and $ReO_2F_3{\cdot}SbF_5$[8] except that the Re−F_t bonds of $Re_2O_2F_9^+$ are shorter than those of $ReO_2F_3{\cdot}SbF_5$.

The bond valences for individual bonds, as defined by Brown,[41−43] are given in Table 2. The total bond valences for the Tc atoms are 7.06 and 6.98 vu, with average contributions of 2.01 vu/oxygen atom, 1.12 vu/terminal fluorine atom, and 0.53 vu/bridging fluorine atom. The values for the Tc−O and Tc−F_t indicate that these bonds have the greatest covalent character observed to date for a technetium(VII) oxofluoride, which is consistent with the expected increase in electronegativity of the metal with decreasing number of oxo ligands. The bond valence value for the bridging Tc−F_b bond approaches 0.50 vu and is in accord with equal sharing of the bridging fluorine between the $TcOF_4$ units of the cation.

The octahedra formed by the light atoms in $Tc_2O_2F_9^+$ are relatively undistorted, having average O···F_t, F_t···F_t, and F_t···F_b distances of 2.584(7), 2.504(5), and 2.538(6) Å, respectively. The bending of the terminal fluorines away from the oxygen is in agreement with the predictions of the VSEPR model[27] and arises from the greater spatial requirement of the oxygen double bond pair domain and its repulsive interaction with the Tc−F single bond pair domains at approximately right angles to it. The average O−Tc−F_t angle is 98.0(3)° and is in excellent agreement with the averages of the corresponding angles in $W_2O_2F_9^-$ (99(2)°),[36] $Re_2O_2F_9^+$ (98(2)°),[15] and $V_2O_2F_8(H_2O)^{2-}$ (99.9(2)°).[38] The symmetry-inequivalent $TcOF_4$ groups of the $Tc_2O_2F_9^+$ cation adopt an eclipsed conformations (dihedral angles between the [O, F_e, Tc, F_e, F_b] planes average 0.55°) as observed in the structures of $[Re_2O_2F_9][Sb_2F_{11}]$[15] and $Mo_2O_2F_9^{3-}$,[37] but contrasts with the staggered conformation adopted by $W_2O_2F_9^-$ [36] and $V_2O_2F_8(H_2O)_2^-$ [38] and the energy-minimized, staggered conformation predicted by theory (see the Computational Results). The Tc−F_b−Tc (158.2(2)°) bridge angle and that in the rhenium analogue (170(3)°) indicate that the packing of the fluorine atoms in both salts is intermediate with respect to the ideal hexagonal (132°) and cubic (180°) closest packed values.[44]

(c) Solution NMR Spectroscopic Characterization of $TcOF_5$ Adducts of PnF_5 (Pn = As, Sb). Both $[Tc_2O_2F_9][AsF_6]$ and $[Tc_2O_2F_9][Sb_2F_{11}]$ are sparingly soluble in anhydrous HF at 25 °C and are insoluble at lower temperatures. Attempts to dissolve the solids in SO_2ClF resulted in rapid decomposition at the melting point of the solvent accompanied by the formation of intense blue colored solutions changing to red. The ^{19}F NMR spectrum of $[Tc_2O_2F_9][AsF_6]$ in HF at 30 °C consists of a single broad resonance at −191.9 ppm ($\Delta\nu_{1/2}$ = 280 Hz) assigned to HF undergoing fluorine exchange with AsF_6^- and F-on-Tc^{VII}. The ^{99}Tc NMR spectrum of this solution at 30 °C consists of a broad resonance at 300.8 ppm ($\Delta\nu_{1/2}$ = 300 Hz) and is shielded with respect to $TcOF_5$ (394.5 ppm), which is consistent with the observed shielding of the ^{99}Tc nucleus in going from $TcO_2F_4^-$ (247.4 ppm)[7] to "$TcO_2F_2^+$" (140.3 ppm).[8] No $^1J(^{99}Tc-^{19}F)$ coupling to the fluorines could be resolved because of the fast quadrupolar relaxation of the ^{99}Tc nucleus and/or fluorine exchange. The ^{19}F NMR spectrum of a solution of $[Tc_2O_2F_9][Sb_2F_{11}]$ in HF at 30 °C consists of exchange-broadened resonances at 403.4 ppm ($\Delta\nu_{1/2}$ = 1200 Hz) assigned to F-on-Tc^{VII} and at −120.3 ppm ($\Delta\nu_{1/2}$ = 8000 Hz) assigned to $SbF_6^-/Sb_2F_{11}^-$ and a singlet at −198.1 ppm ($\Delta\nu_{1/2}$ = 50 Hz) assigned to HF solvent. No signal was observed that could be assigned to the bridging fluorine of the $Tc_2O_2F_9^+$ cation. The ^{99}Tc NMR spectrum of this solution at 30 °C consists of a broad resonance at 288.0 ppm ($\Delta\nu_{1/2}$ = 960 Hz). The ^{19}F exchange behavior of $[Tc_2O_2F_9][AsF_6]$ and $[Tc_2O_2F_9][Sb_2F_{11}]$ in HF solution indicates that the $Tc_2O_2F_9^+$ cation is likely involved in a dissociative equilibrium. The observation of a F-on-Tc^{VII} resonance in the ^{19}F NMR spectrum of the $Sb_2F_{11}^-$ salt where a separate resonance was not observed for the AsF_6^- salt at the same temperature is consistent with the slower exchange rate anticipated as a result of the higher acidity that HF solvolysis

(36) Hoskins, B. F.; Linden, A.; O'Donnell, T. A. *Inorg. Chem.* **1987**, *26*, 2223.
(37) Leimkühler, M.; Buchholz, N.; Mattes, R. *Z. Naturforsch.* **1989**, *44b*, 389.
(38) Hilbers, M.; Leimkühler, M.; Mattes, R. *Z. Naturforsch.* **1989**, *44b*, 383.
(39) Davies, C. G.; Gillespie, R. J.; Ireland, P. R.; Sowa, J. M. *Can. J. Chem.* **1974**, *52*, 2048.
(40) McKee, D. E.; Zalkin, A.; Bartlett, N. *Inorg. Chem.* **1973**, *12*, 1713.
(41) Brown, I. D. *J. Solid State Chem.* **1974**, *11*, 214.
(42) Brown, I. D. In *Structure and Bonding in Crystals*; O'Keefe, M., Navrotsky, A., Eds.; Academic Press: London, 1981; Vol. 2, p 1.
(43) Brown, I. D.; Altermatt, D. *Acta Crystallogr.* **1985**, *B41*, 244.
(44) Edwards, A. J.; Jones, J. R. *J. Chem. Soc A* **1968**, 2074.

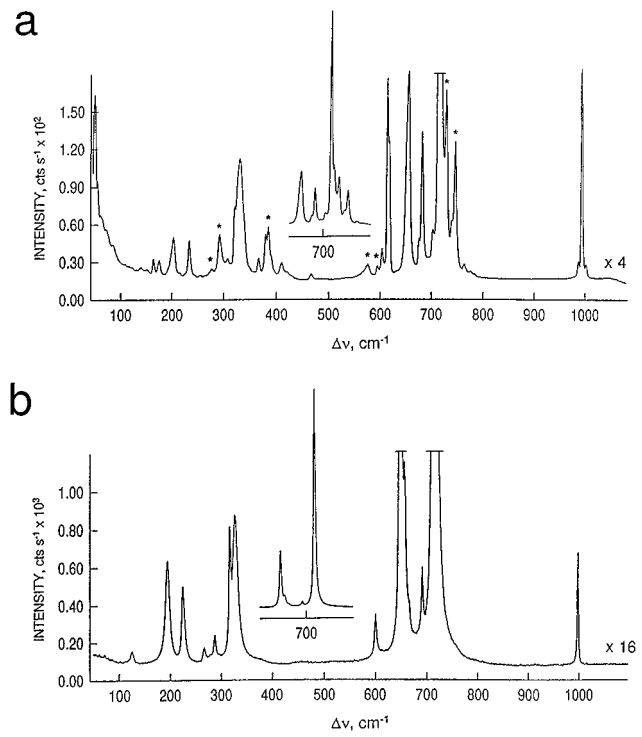

Figure 6. Raman spectra (514.5 nm excitation) of (a) microcrystalline $[Tc_2O_2F_9][AsF_6]$ at −150 °C using (asterisks denote FEP sample tube lines) and (b) a randomly orientated single crystal of $[Tc_2O_2F_9][Sb_2F_{11}]$ recorded in a glass Lindemann capillary at 22 °C.

of the $Sb_2F_{11}^-$ anion imparts to the solvent medium. The low solubilities of the salts at low temperatures prevented the pursuit of variable-temperature NMR studies with the view to slow the exchange.

The ^{19}F NMR spectrum of $TcOF_5$ dissolved in liquid SbF_5 at 50 °C consists of a singlet in the F-on-Tc^{VII} region at 414.2 ppm ($\Delta\nu_{1/2}$ = 180 Hz) and broad lines at −89 (shoulder), −104.5 ($\Delta\nu_{1/2} \approx$ 8800 Hz), and −129.4 ($\Delta\nu_{1/2} \approx$ 5700 Hz) ppm corresponding to $Sb_nF_{5n+1}^-/(SbF_5)_n$. The ^{99}Tc resonance could not be obtained at 50 °C because of quadrupole collapse of the resonance into the spectral baseline as a result of the long molecular correlation time of the technetium(VII) species that results from the high viscosity of SbF_5. The singlet ^{19}F resonance is consistent with the formation of the $TcOF_4^+$ cation, which, like isoelectronic $MoOF_4$,[16] is expected to have a square pyramidal structure (see the Computational Results) and a single equatorial fluorine environment. The ^{19}F-on-Tc^{VII} chemical shift in SbF_5 is only slightly more deshielded than that resulting when $[Tc_2O_2F_9][Sb_2F_{11}]$ is dissolved in HF, suggesting that the latter salt may be primarily dissociated into $TcOF_4^+$ and SbF_6^- anions in HF solvent. The large decrease in the ^{19}F shielding (108 ppm in SbF_5; 97.5 ppm in HF) with respect to the weighted average ^{19}F chemical shift of $TcOF_5$ in HF (305.9 ppm; 30 °C) is also consistent with the formation of the $TcOF_4^+$ cation in both solvent media.

(d) Characterization of $[Tc_2O_2F_9][AsF_6]$ and $[Tc_2O_2F_9][Sb_2F_{11}]$ by Raman Spectroscopy. The Raman spectra of both $Tc_2O_2F_9^+$ salts are shown in Figure 6. The observed frequencies and their assignments are listed in Table 5. The spectral assignments were based on C_{2v} symmetry (eclipsed conformation) for the free cation in the crystal structure and C_1 symmetry (staggered conformation) for the energy-minimized gas-phase cation. Group theory predicts 33 Raman- and infrared-active vibrational modes for either symmetry.

A factor-group analysis was carried out to evaluate the degree of vibrational coupling within the unit cell of $[Tc_2O_2F_9][Sb_2F_{11}]$. The factor-group analysis is summarized in the Supporting Information. Neither splittings arising from coupling within the unit cell nor splittings arising from coupling between the $OTcF_4$ groups of the cation and the SbF_5 groups of the anion were resolved. The assignment of the Raman spectrum of the $Tc_2O_2F_9^+$ cation was assisted by comparison with those of $TcOF_5$ and by LDFT calculations of the frequencies (see the Computational Results), which predict that the $TcOF_4$ groups are weakly coupled. Consequently, individual experimental frequencies are often described in terms of two coupled components in Table 5. The previously reported Raman spectrum of the $Re_2O_2F_9^+$ cation has been reassigned using frequencies and more detailed mode descriptions derived from LDFT calculations and are compared with those of the technetium analogue in Table 5.

The Tc−O and equatorial Tc−F stretching modes of $Tc_2O_2F_9^+$ are shifted to high frequency relative to the corresponding modes in $TcOF_5$, reflecting an increase in the covalent character of these bonds resulting from the partial removal of the axial fluorine from $TcOF_5$. The out-of-phase bridging $Tc-F_b-Tc$ stretching mode is expected to be very weak and broad by analogy with the spectra of other fluorine-bridged species, i.e., $MO_2F_3{\cdot}PnF_5$ (M = Tc, Re; Pn = As, Sb), $Re_2O_4F_7^-$, and $Os_2O_4F_7^+$ [11] and was accordingly assigned to the weak, broad band at 458 [467] cm^{-1} ($[Tc_2O_2F_9][Sb_2F_{11}]$ frequencies with $[Tc_2O_2F_9][AsF_6]$ frequencies in square brackets). The in-phase component, predicted at 126 cm^{-1}, is expected to be stronger than the asymmetric component and is assigned to the band at 128 [137] cm^{-1}.

The vibrational assignments of the $Sb_2F_{11}^-$ anion and of the AsF_6^- anion are in agreement with previously reported values for $Sb_2F_{11}^-$ [45,46] and an undistorted AsF_6^- [33,47,48] anion of O_h point symmetry.

Computational Results

We have previously shown that the geometries of transition-metal-containing oxygen and fluorine ligands can be reliably predicted at the local density functional theory level.[7,8,10−12,49,50]

MOF_5 (M = Tc, Re, Os). The molecular geometry of $TcOF_5$ was optimized at the local density theory (LDFT) level with a polarized double-ζ basis set (DZVP) and a polarized triple-ζ basis set (TZ94P). The calculated structure of $TcOF_5$ (Table 6) has C_{4v} point symmetry with a Tc−O bond distance of 1.703 (1.693) Å (DZVP value given, with TZ94P value in parentheses), a $Tc-F_e$ bond length of 1.858 (1.845) Å, and a $Tc-F_a$ bond length of 1.891 (1.883) Å. The global geometry is in excellent agreement with the observed one; in particular the $Tc-F_a$ bond is found to be significantly longer than the $Tc-F_e$ bonds, and the equatorial fluorines are bent away from the axial oxygen to a greater extent than in the disordered structure (see the X-ray Crystal Structure of $TcOF_5$). Geometric parameters were also calculated for the isostructural $ReOF_5$ and $OsOF_5$ molecules (Table 6), which exhibit similar trends.

(45) Gillespie, R. J.; Landa, B.; Schrobilgen, G. J. *Inorg. Chem.* **1976**, *15*, 1256.
(46) Gillespie, R. J.; Landa, B. *Inorg. Chem.* **1973**, *12*, 1383.
(47) Gillespie, R. J.; Schrobilgen, G. J. *Inorg. Chem.* **1974**, *13*, 1230.
(48) Christe, K. O.; Charpin, P.; Soulie, E.; Bougon, R.; Fawcett, J.; Russell, D. R. *Inorg. Chem.* **1984**, *23*, 3756.
(49) Sosa, C.; Andzelm, J.; Elkin, B. C.; Wimmer, E.; Dobbs, K. D.; Dixon, D. A. *J. Phys. Chem.* **1992**, *96*, 6630.
(50) Parr, R. G.; Yang, W. *Density-Functional Theory of Atoms and Molecules*; Oxford University Press: New York, 1989.

Table 5. Observed and Calculated Vibrational Frequencies (cm^{-1}),[a] Assignments, and Mode Descriptions for $Tc_2O_2F_9^+$ and $Re_2O_2F_9^+$ at the LDFT Level

frequencies (cm^{-1})					
$Tc_2O_2F_9^+$			$Re_2O_2F_9^+$		
exptl[a]			exptl[a]		
$Tc_2O_2F_9^+Sb_2F_{11}^-$	$Tc_2O_2F_9^+AsF_6^-$	LDFT[b]	$Re_2O_2F_9^+Sb_2F_{11}^-$	LDFT[b]	assignment[c]
998 (4)	1007 (1), 998 (28)	1024.6 (6)		1076.1 (5)	ν_{sym}(M−O)
			1059 (53)		
	992 (2)	1013.6 (234)		1069.7 (163)	ν_{as}(M−O)
		756.0 (275)		750.8 (276)	(MF_{1e} − MF_{3e}) + ($M'F_{4e}$ − $M'F_{2e}$)
	722 (28), sh		762 (100)		
		755.6 (265)		751.4 (252)	($M'F_{1e}$ − $M'F_{3e}$) + (MF_{2e} − MF_{4e})
		744.0 (0)		739.5 (2)	(MF_{1e} − MF_{3e}) − ($M'F_{4e}$ − $M'F_{2e}$)
717 (100)	717 (100)		691 (31)		
		743.2 (11)		738.0 (33)	($M'F_{1e}$ − $M'F_{3e}$) − (MF_{2e} − MF_{4e})
		703.1 (49)		747.9 (31)	(MF_4 sym − $M'F_4$ sym) + ν_{as}(MF_bM')
	706 (6)		698 (18)		
		696.0 (0)		741.5 (11)	$M'F_4$ sym + MF_4 sym
		646.1 (0)		685.4 (0)	MF_4 sym − $M'F_4$ sym
657 (6)	659 (24)		657 (39)		
		645.9 (0)		685.8 (0)	$M'F_4$ sym − MF_4 sym
458 (<1), br	467 (<1)	483.6 (309)		487.4 (300)	ν_{as}(MF_bM')
	339 (7), sh	319.9 (0)			TcF_bTc' + $F_{4e}TcO$ + $F_{3e}Tc'O$
				343.3 (0)	$OReF_{4e}$ + $ORe'F_{4e}/F_{3e}$ (bisects) + bend at F_b
			341 (48)		
				340.0 (1)	$OReF_{1e}$ + $ORe'F_{3e}/F_{2e}$ (bisects) + bend at F_b
331 (5)	331 (14)	317.6 (3)			$F_{1e}Tc'O$ + $F_{3e}TcO$
321 (4)	321 (8), sh	308.8 (0)			$F_{1e}TcO$ + $F_{4e}Tc'O$ (bisects $F_{4e}Tc'F_{1e}$)
		307.9 (0)		335.8 (0)	$F_{4e}MF_{1e}$ + $F_{2e}MF_{3e}$
				327.5 (0)	$OReF_{3e}$ − $ORe'F_{3e}/F_{2e}$ (bisects)
				325.2 (1)	$OReF_{4e}$ − $ORe'F_{4e}/F_{3e}$ (bisects)
		307.7 (0)			$F_{2e}TcO$ + $F_{1e}Tc'O$ + some asym umbrella
		305.5 (3)	304 (8)	301.5 (5)	MF_4 umbrella + $M'F_4$ umbrella
		301.8 (1)		321.3 (0)	$F_{3e}M'F_{2e}$ + $F_{1e}M'F_{4e}$
		289.4 (27)			$OTc'F_b$ + $OTcF_b$ (has TcF_bTc' bend) in-plane
		282.5 (25)			$OTc'F_b$ + $OTcF_b$
				283.5 (31)	ReF_bRe' in-plane
			272 (4)		
				276.0 (31)	ReF_bRe' out-of-plane
269 (1)	253 (<1)	252.9 (178)			(TcF_4 umbrella − $Tc'F_4$ umbrella) + ν_{as}(TcF_bTc')
				255.6 (147)	ReF_4 umbrella − $Re'F_4$ umbrella
			230 (14)	226.2 (0)	$F_{4e}ReF_{2e}$ in-plane bend − $F_{4e}Re'F_{2e}$ in-plane bend
				223.2 (1)	$F_{1e}ReF_{3e}$ in-plane bend − $F_{1e}Re'F_{3e}$ bend
228 (3)	233 (4)	217.8 (0)			$F_{4e}TcF_{2e}$ bend − $F_{1e}Tc'F_{3e}$ bend (out-of-plane)
198 (3)	202 (5)	213.3 (0)			$F_{3e}TcF_{1e}$ bend − $F_{4e}Tc'F_{2e}$ bend (out-of-plane)
			212 (7)	210.9 (0)	asym umbrella at Re
				197.8 (0)	asym umbrella at Re′
				188.8 (5)	ReF_bRe' + $F_{2e}Re'F_{4e}$ + $F_{1e}ReF_{3e}$
	173 (2)	182.4 (1)			$F_{3e}TcF_{1e}$ bend − $F_{4e}TcF_{2e}$ bend (in-plane)
				181.2 (3)	ReF_bRe' + $F_{2e}Re'F_{4e}$ + $F_{2e}ReF_{4e}$
	162 (2)	177.3 (4)			$F_{3e}TcF_{1e}$ bend + $F_{1e}Tc'F_{3e}$ bend (out-of-plane)
		174.4 (1)			$F_{2e}Tc'F_{4e}$ bend − $F_{1e}Tc'F_{3e}$ bend (in-plane)
		167.9 (3)			$OTcF_b$ bend + $OTcF_b$ bend out-of-plane + $F_{2e}Tc'F_{4e}$ bend + $F_{4e}TcF_{2e}$
128 (1)	137 (1)	125.6 (1)		116.2 (0)	ν_{sym}(MF_bM') + some OMF_b bend − OMF_b bend in-plane
				123.2 (0)	$ReOF_4$ group rock (toward F_b) + $ReOF_4$ group rock (toward F_b)
			134 (2)		
				122.9 (0)	$ReOF_4$ group rock (toward F_b) − $ReOF_4$ group rock (toward F_b)
		115.7 (0)			$OTcF_b$ bend − $OTcF_b$ bend out-of-plane
	82 (4)				
		110.6(1)			$OTcF_b$ bend − $OTcF_b$ bend in-plane
				54.1 (0)	(F_4O group)ReF_bRe'(OF_4 group) bend in-plane
	59 (7)	50.0 (1)			TcF_bTc' bend in-plane
				48.2 (0)	(F_4O group)ReF_bRe'(OF_4 group) bend out-of-plane
	48 (21)	43.8 (0)		39.2 (0)	torsion of MF_4 about the MF_b bonds
		34.4 (1)			TcF_bTc' bend out-of-plane

[a] The following anion peaks were also observed and are assigned to $Sb_2F_{11}^-$ [$Tc_2O_2F_9^+$, 692 (3), 666 (2),sh, 650 (26), 601 (2), 291 (1); $Re_2O_2F_9^+$: 606 (9), 579 (4),br, 283 (6); taken from ref 15] and to AsF_6^- [$Tc_2O_2F_9^+$, $\nu_1(A_{1g})$, 685 (17); $\nu_2(E_g)$, 547 (<1), br, $\nu_5(T_{2g})$ 366 (2)]. [b] Infrared intensities, km mol^{-1}, are given in parentheses. [c] The point symmetry is taken as C_{2v} (eclipsed) for the experimental geometry of the $Tc_2O_2F_9^+$ cation, whereas it is C_1 for the energy-minimized (staggered) geometry of the gas-phase cation (see Computational Results). The fluorine atom labeling scheme is F_b, bridging fluorine; F_{1e}, F_{2e}, F_{3e}, and F_{4e}, fluorine atoms cis to the O; F_{1e}, F_{3e}, and F_{2e}, F_{4e} pairs, trans to each other.

Table 6. Calculated (LDFT) Geometric Parameters, Atomic Charges, Mayer Valencies, and Mayer Bond Orders for $TcOF_5$, $ReOF_5$, and $OsOF_5$ and Geometric Parameters Observed for $TcOF_5$

Geometric Parameters

	$TcOF_5$			$ReOF_5$			$OsOF_5$		
	exptl	TZ94P	DZVP	TZP/PP	DZVP2/PP	DZVP2/PP	TZP/PP	DZVP2/PP	DZVP2/LANL
M−O	1.67(1)	1.693	1.702	1.718	1.712	1.698	1.716	1.709	1.694
M−F_a	1.90(1)	1.883	1.894	1.920	1.916	1.892	1.908	1.899	1.876
M−F_e	1.81(1)	1.845	1.858	1.871	1.865	1.845	1.895	1.882	1.868
O−Tc−F_e		94.3	94.3	94.0	94.1	94.5	94.4	94.6	95.0
F_a−Tc−F_e		85.7	85.7	86.0	85.9	85.5	85.6	85.4	85.0
F_e−Tc−F_e	176.4(5)	171.3	171.4	172.1	171.8	170.9	171.2	170.8	169.9
		89.7	89.7	89.7	89.7	89.6	89.7	89.6	89.5

Atomic Charges and Mayer Valencies[a]

	$TcOF_5$		$ReOF_5$			$OsOF_5$		
	TZ94P	DZVP	TZP/PP	DZVP2/PP	DZVP2/LANL	TZP/PP	DZVP2/PP	DZVP2/LANL
M	2.11	1.28 [6.43]	2.42	2.00	1.76 [6.13]	1.87	1.99	1.72 [6.12]
O	−0.25	−0.12 [2.59]	−0.38	−0.30	−0.26 [2.40]	−0.13	−0.25	−0.22 [2.43]
F_e	−0.36	−0.22 [1.27]	−0.39	−0.33	−0.29 [1.13]	−0.39	−0.35	−0.30 [1.11]
F_a	−0.42	−0.26 [1.21]	−0.48	−0.39	−0.35 [1.05]	−0.34	−0.35	−0.31 [1.11]

$Tc_2O_2F_9^+$ (DZVP)[c]

Tc(1)	1.41 [6.23]	Tc(2)	1.40 [6.25]	F(4)	−0.47 [0.82]	O(1)	−0.03 [2.66]
O(2)	−0.03 [2.66]	F(2A)	−0.17 [1.36]	F(1)	−0.16 [1.37]	F(2)	−0.15 [1.38]
F(5)	−0.15 [1.38]	F(6A)	−0.17 [1.36]	F(6)	−0.15 [1.38]		
F(3)	−0.16 [1.37]						

Mayer Bond Orders[b]

$TcOF_5$	Tc−O	1.95	Tc−F_e	0.91	Tc−F_a	0.83
$ReOF_5$	Re−O	1.90	Re−F_e	0.87	Re−F_a	0.76
$Tc_2O_2F_9^+$	Tc(1)−F(4)	0.30	Tc(2)−F(4)	0.30	Tc(1)−O(1)	2.04
	Tc(2)−O(2)	2.04	Tc(1)−F(2A)	0.97	Tc(1)−F(1)	0.98
	Tc(1)−F(2)	0.98	Tc(1)−F(3)	0.98	Tc(2)−F(5)	0.98
	Tc(2)−F(6A)	0.97	Tc(2)−F(7)	0.97	Tc(2)−F(6)	0.98

[a] Mayer valencies are given within brackets. [b] The Mayer bond orders for $OsOF_5$ could not be calculated. [c] See Table 2 for the experimental and calculated geometrical parameters of $Tc_2O_2F_9^+$.

The calculated vibrational frequencies for $TcOF_5$ are compared with the experimental values in Table 3. No scaling of the stretching frequencies was applied. The frequencies obtained with the two different basis sets are essentially the same and are in good agreement with experiment. As observed previously in calculations on technetium, rhenium, and osmium oxide fluorides, the largest discrepancies are for the modes involving O atoms. For comparison, the calculated vibrational frequencies of $ReOF_5$ and $OsOF_5$ (DZVP2/LANL-ECP basis set) are listed in Table 4. They are also in very good agreement with the experimental values and are similar to those of $TcOF_5$. The biggest difference is that the two lowest E bending frequencies for $ReOF_5$ are below the experimental values by about 15−20 cm^{-1} and the B_2 mode and two of the E bending modes for $OsOF_5$ are predicted to be lower than the experimental values by up to 40−100 cm^{-1}. In the cases of $OsOF_5$ and $ReOF_5$, the frequencies at 263 and 367 cm^{-1} and at 260 and 367 cm^{-1} have been reassigned to ν_{10}(E) and ν_9(E), respectively.

The calculated atomic charges and Mayer valencies[51] are given in Table 6. The DZVP charges show that the Tc in $TcOF_5$ has a charge of +1.28e just as in TcO_2F_3 and negative charges of −0.12 e on O and −0.22 e and −0.26 e on F_e and F_a, respectively. The Mayer valencies show a valency of 6.43 for Tc with valencies of 2.59 for O and 1.27 and 1.21 for F_e and F_a, respectively. The Mayer bond order (Table 6) is 1.95 for the Tc−O bond, showing that this bond is essentially a double bond, whereas the Tc−F bond orders of 0.91 for F_e and 0.83 for F_a show these bonds to be slightly less than a single bond. We note that the bond orders for Tc−F_e and Tc−F_a are in agreement with the calculated and experimental bond lengths and the internal stretching force constants determined in this study. The same correlations occur between the M−F_e and M−F_a stretching force constants of $ReOF_5$ and $OsOF_5$ and their calculated Mayer bond orders and bond lengths. The calculations also show that the metals in $ReOF_5$ and $OsOF_5$ are more electronegative, with more positive charge on the metal and more negative charge on the light atoms (Table 6). This is reflected in their Mayer bond orders, which, although similar to those of $TcOF_5$, are generally smaller.

The fluoride ion affinities (FA's) of $TcOF_5$ (76.4 kcal mol^{-1}) and $ReOF_5$ (77.9 kcal mol^{-1}), as defined in ref 12, have been determined at the LDFT level using DZVP and DZVP2/ECP basis sets, respectively. The FA values are similar to each other and to those determined for TcO_2F_3 and ReO_2F_3.[12] The established existence of the $ReOF_6^-$ anion[52,53] and the similarities of the FA values of their parent molecules suggest that it may be possible to prepare salts of the $TcOF_6^-$ anion.

$M_2O_2F_9^+$ (M = Tc, Re). The calculations on the fluorine-bridged $M_2O_2F_9^+$ cations were done as described above for the monomers (Table 6 and Supporting Information). There is very good agreement between the experimental and calculated geometries, even though the calculated bond lengths are slightly longer. However, and contrary to their X-ray structures, the two

(51) Mayer, I. *Chem. Phys. Lett.* **1983**, *97*, 270; *Theor. Chim. Acta* **1985**, *67*, 315; *Int. J. Quantum Chem.* **1986**, *29*, 73, 477.

(52) Selig, H.; Karpas, Z. *Isr. J. Chem.* **1971**, *9*, 53.

(53) Giese, S.; Seppelt, K. *Angew. Chem., Int. Ed. Engl.* **1994**, *33*, 461; *Angew. Chem.* **1994**, *106*, 473.

Table 7. Calculated Geometrical Parameters and Vibrational Frequencies for MOF_4^+ (M = Tc, Re) (C_{4v})

bond lengths (Å) and bond angles (deg)			frequencies[a]		
	Tc	Re	Tc	Re[b]	assignment
M−F	1.819	1.810	1058 (37)	1092 (29) [1060.0]	A_1, ν(MO)
M−O	1.655	1.658	729 (13)	768 (16) [765.5]	A_1, $\nu_{sym}(MF_4)$
F−M−F	86.3	86.4	256 (6)	237 (5) [232.0]	A_1, MF_4 inversion
F−M−O	104.6	104.6	667 (0)	703 (0)	B_1, $\nu_{as}(MF_4)$
			91 (0)	83 (0)	B_1, FMF−FMF
			345 (0)	357 (0) [340.0]	B_2, δ(FMF)
			780 (252)	770 (254) [696.0]	E, $\nu_{as}(MF_4)$
			296 (7)	301 (2) [294.0]	E, δ(OMF)
			236 (26)	239 (31) [212.5]	E, δ(FMF)

[a] Infrared intensities, km mol^{-1}, are given in parentheses. [b] Values in square brackets are experimental values taken from ref 15.

groups of equatorial F atoms are not eclipsed but staggered with dihedral angles very close to 45°. Thus, one plane approximately eclipses the plane defined by M−F_b−M, and the other is rotated by 44.7° (Tc) and 44.8° (Re). The eclipsed structure for $M_2O_2F_9^+$ with both groups rotated by about 45° with respect to the plane defined by M−F_b−M is not a minimum with two imaginary frequencies, and is only 0.45 kcal mol^{-1} higher in energy for $Tc_2O_2F_9^+$ than the staggered structure. Thus, it is not surprising that crystal packing forces could easily lead to a slightly different structure involving only torsion about the M−F_b bond. It is also worth noting that the calculated M−F_b−M angles are in very good agreement with the observed ones even though it has been shown that these angles can be very dependent on the packing. As expected, there is overall good agreement between the calculated and observed frequencies for the binuclear cations, but assignments for the lower frequency modes are somewhat arbitrary.

The formation of the fluorine-bridged binuclear cation leads to the expected changes. The charges on the Tc (Re) atoms increase from +1.28 (+1.76) e to +1.41 (+1.87) e, and the bridging F has a high negative charge of −0.48 (−0.60) e. As a consequence and to accommodate the overall positive charge, the other atoms reduce their negative charges to −0.03 (−0.14) e for O and −0.15 (−0.22) e to −0.17 (−0.24) e at the other fluorines. The valencies show significant changes at the fluorines. The bridging F has a valency of 0.82 (0.34), whereas the valencies of the terminal atoms increase to 1.37 (1.24). The valencies on the oxygens increase slightly to 2.66 (2.53). The changes in the bond orders reflect the changes in the valencies. The M−F_b bond orders are only 0.30 (0.15), consistent with a weak interaction of the MOF_4^+ moieties with an F^- anion. As expected for the cations, the terminal M−O and M−F bond orders increase relative to those in the neutral MOF_5 molecules.

MOF_4^+ (M = Tc, Re). We also report the geometrical parameters and vibrational frequencies for the MOF_4^+ cations (Table 7). The geometries of both Tc and Re cations are expected to be very similar, with calculated M−O and M−F bonds that are shorter than the M−O and terminal M−F bonds in MOF_5 and $M_2O_2F_9^+$ and with a F−M−O angle that deviates more from 90° than that in either MOF_5 or $M_2O_2F_9^+$. The vibrational spectra are also predicted to be very similar, and as expected, the MO stretching frequencies are found to be shifted to higher frequencies than in the MOF_5 compounds. The calculated values for $ReOF_4^+$ were used to confirm an earlier assignment of the $[ReOF_4][AsF_6]$ salt.[15]

NMR Chemical Shifts. It is now possible to calculate NMR chemical shifts by ab initio theoretical methods. We have used three different approaches all within the density functional theory formalism (Table 8). First we have used the IGLO[54,55] and LORG[56] treatments of the gauge invariance problem in an uncoupled DFT approach[57] as well as the GIAO approach.[58−61] The standards used for the relative chemical shift calculations are: TcO_4^- for ^{99}Tc, $CFCl_3$ for ^{19}F, and H_2O for ^{17}O. The relative chemical shift of ^{99}Tc in $TcOF_5$ is calculated to be 632 and 587 ppm at the DZVP/IGLO and DZVP/LORG levels, respectively, and 556 and 551 ppm at the TZVP/IGLO and TZVP/LORG levels, respectively. With the larger TZ2P basis set, the shift is predicted to be 676 ppm at the GIAO level. The difference from experiment (Table 8) could be due to the need for a better basis set or for the need to include relativistic effects. The chemical shifts for F_e, F_a, and O were calculated for both $TcOF_5$ and $ReOF_5$. The calculated chemical shifts for the fluorines are also too high when compared with the experimental values, although the difference between the axial and equatorial fluorines is correctly predicted to be about 300 (Tc) and 220 (Re) ppm, and F_e is found to be more deshielded than F_a. Note that the experimental difference is strongly dependent on temperature and solvent. Our calculated values correspond to 0 K, so it is probably most appropriate to compare to the lower

Table 8. NMR Shifts (ppm) for $TcOF_5$, $ReOF_5$, $TcOF_4^+$, and $ReOF_4^+$

$TcOF_5$

	TZVP		DZVP		TZ2P	
atom	LORG	IGLO	LORG	IGLO	GIAO	exptl
Tc	556	551	632	587	676	394.5,[a] 433.8[b]
F_a	85	64	201	304	185.5	45.0,[a] 62.0[c]
F_e	353	308	452	535	485.6	371.7,[a] 364.1[c]
Δ[d]	268	244	251	231	300.1	326.7,[a] 302.1[c]
O					1173	1211[e]

$ReOF_5$			$TcOF_4^+$		$ReOF_4^+$	
	TZ2P			TZ2P		TZ2P
atom	GIAO	exptl[f]	atom	GIAO	atom	GIAO
F_a	30.2	−36.0	Tc	305.1		
F_e	255.6	183.4	F	558.3	F	294.2
Δ[d]	225.4	219.4	O	1141.4	O	894.9
O	944.8					

[a] Recorded in HF at 35 °C. [b] Recorded in SO_2ClF at 30 °C. [c] Recorded in SO_2ClF at −110 °C. [d] $\Delta = \delta(^{19}F_e) - \delta(^{19}F_a)$. [e] Recorded in HF at 25 °C (ref 5). [f] Recorded in HF at 30 °C.

(54) Kutzelnigg, W. *Isr. J. Chem.* **1980**, *19*, 193.
(55) Schindler, M. and Kutzelnigg, W., *J. Chem. Phys.* **1982**, *76*, 1919.
(56) Hansen, A. E.; Bouman, T. D. *J. Chem. Phys.* **1985**, *82*, 5035.
(57) Arduengo, A. J. III; Dixon, D. A.; Kumashiro, K. K.; Lee, C.; Power, W. P.; Zilm, K. W. *J. Am. Chem. Soc.* **1994**, *116*, 6361.
(58) Cheeseman, J. R.; Trucks, G. W.; Keith, T. A.; Frisch, M. J. *J. Chem. Phys.* **1996**, *104*, 5497.
(59) London, F. *J. Phys. Radium (Paris)* **1937**, *8*, 397.
(60) Ditchfield, R. *Mol. Phys.* **1974**, *27*, 789.
(61) Wolinski, K.; Hinton, J. F.; Pulay, P. *J. Am. Chem. Soc.* **1990**, *112*, 8251.

temperature result. The ^{17}O chemical shift for $TcOF_5$ is predicted to be 1173 ppm at the GIAO/TZ2P level, which is in good agreement with the observed value of 1211 ppm.

The ^{19}F and ^{99}Tc chemical shifts were also calculated for $TcOF_4^+$ and $ReOF_4^+$. For $TcOF_4^+$, the calculated chemical shift was too high when compared to the experimental value (403.4 ppm in HF solvent and 414.2 ppm in SbF_5 solvent); however, the deshielding of the ^{19}F signal in going from $TcOF_5$ to $TcOF_4^+$, which was observed experimentally, was reproduced for both the technetium and rhenium cases.

Conclusion

The last member of the technetium(VII) oxofluoride series, $TcOF_5$, has been synthesized by the reaction of TcO_2F_3 with KrF_2 in anhydrous HF and is the fourth known neutral oxide pentafluoride, the others being $ReOF_5$, $OsOF_5$, and IOF_5. The volatile orange solid adopts the expected pseudooctahedral (C_{4v}) geometry as determined experimentally in the gas phase, solution, and solid state and theoretically by LDFT calculations. Of the known oxide pentafluorides, the technetium and iodine compounds are presently the only neutral oxide pentafluorides for which accurate experimental structures are known. The lengthening of the axial Tc−F bond resulting from the trans influence of the oxo ligand was observed experimentally for $TcOF_5$ in the X-ray crystal structure, and its significantly greater ionic character was also inferred from relative ^{19}F NMR chemical shifts and line widths, Tc−F bond valence values, and Mayer bond orders. The elongation of the metal−axial fluorine bond length and lower bond order relative to that of the equatorial fluorine were also confirmed by LDFT calculations for $TcOF_5$, $ReOF_5$, and $OsOF_5$. The internal stretching force constants obtained for $TcOF_5$, $ReOF_5$, and $OsOF_5$ by ab initio methods indicate that the axial M−F stretching force constants are less than the equatorial ones, and are in agreement with structural and spectroscopic findings.

The fluoride ion donor behavior of $TcOF_5$ was investigated and resulted in the syntheses of the AsF_6^- and $Sb_2F_{11}^-$ salts of the binuclear $Tc_2O_2F_9^+$ cation. The cation consists of two fluorine-bridged $TcOF_5$ units, and also manifests the trans influence of the oxo ligand by location of the more ionic bridging fluorine trans to the oxo ligands. Solution NMR studies of $TcOF_5$ in strong fluoride ion acceptor media are consistent with the formation of the $TcOF_4^+$ cation, which is predicted by theory to have a square pyramidal geometry.

Further fluorination of $TcOF_5$ was attempted using [KrF]-[AsF_6] in HF; however, no evidence was obtained for the formation of the TcF_6^+ cation.

Experimental Section

All operations were conducted in laboratories that were monitored routinely by the McMaster University Health Physics Group for radioactive contamination. All work involving ^{99}Tc was licensed and performed according to the regulations and recommendations of the Canadian Atomic Energy Control Board (CAECB).[62]

Apparatus and Materials. Volatile materials were handled in vacuum lines constructed of FEP and Pyrex, and nonvolatile materials were handled in the dry nitrogen atmosphere of a glovebox, as previously described. The procedures for the preparation of KrF_2,[63] TcO_2F_3,[6] [Cs][TcO_2F_4],[7] XeF_6,[64] and AsF_5,[65] have been described previously. Anhydrous HF (Harshaw Chemical Co.),[66] SbF_3 (Aldrich, 98%),[67] and SbF_5 (Ozark-Mahoning Co.)[68] were dried/purified by the standard literature methods. Fluorine gas (Air Products) was used without further purification.

Caution: Extreme care is required in the disposal of KrF_2 and Xe^{VI} compounds to avoid violent detonations, which could result in the spread of radioactive contamination. Routine disposals of small amounts of HF, KrF_2, XeF_6, and $XeOF_4$ (from the preparation of TcO_2F_3)[6] were carried out by dynamic pumping of these volatile materials through a stainless steel column packed with soda lime. Disposal of the contents of sealed FEP sample tubes containing technetium and KrF_2/Xe^{VI} compounds dissolved in HF was accomplished by freezing the sample in liquid nitrogen, cutting one end of the tube open, and immediately inverting it into a cold aqueous base solution contained inside a stainless steel tube. The tube was immediately covered by inverting a second larger diameter steel tube, sealed at one end and of near equal length, over it and allowing it to stand inside a plastic bucket until the contents of the FEP sample tube had been expelled and hydrolyzed. All disposal operations were carried out behind a protective shield in a fumehood. Solid technetium compounds described in this work were also disposed of in aqueous base. All aqueous solutions containing ^{99}Tc were evaporated and disposed of as radioactive waste in accord with CAECB regulations.[62]

Preparation of $TcOF_5$ and Crystal Growth. In a typical experiment, 0.0658 g (0.350 mmol) of TcO_2F_3 was loaded into a flared $^1/_4$-in. o.d. FEP reactor fitted to a 316 stainless steel Whitey ORF2 valve through a stainless steel $^1/_4$-in. AN nipple. Anhydrous HF (ca. 0.5 mL) was condensed onto the solid. Krypton difluoride (0.33615 g, 2.760 mmol) was sublimed from an FEP weighing vessel into the reactor in three aliquots. The reaction mixture was warmed to room temperature between each addition and periodically sonicated over a period of 24 h until gas evolution ceased. The noncondensable gases were then removed at −196 °C, and additional KrF_2 was condensed into the reactor until the insoluble TcO_2F_3 completely reacted to form a deep orange solution of $TcOF_5$ in HF. The solvent was then removed at −78 °C to yield a volatile orange solid that could be readily sublimed under static vacuum at room temperature. Crystals suitable for X-ray structure determination were grown by sublimation. The bulk sample was initially sublimed, under static vacuum, to the upper portion of a valved $^1/_4$-in. o.d. FEP sample tube, cooled to −78 °C in a dry ice/acetone bath, and then pressurized to 0.5 atm with dry nitrogen. The sample was then partially withdrawn from the bath, whereupon crystals of $TcOF_5$ slowly resublimed to the cooler, lower region of the tube. Once well-defined crystals had formed, the sample tube was pressurized to ca. 1 atm with dry nitrogen, and the crystals were maintained at −78 °C until mounted. The crystals were freed from the walls of the cold vessel by mechanical shocking and mounted as described elsewhere.[69] The crystal used for the data acquisition had the dimensions $0.25 \times 0.10 \times 0.08$ mm^3.

In an attempt to increase the rate of the reaction leading to $TcOF_5$ and to minimize the autodecomposition of KrF_2, [Cs][TcO_2F_4] (0.0514 g, 0.151 mmol) was allowed to react with an excess of KrF_2 in anhydrous HF (ca. 0.35 mL) inside a 4 mm FEP reaction vessel equipped with a Kel-F valve at 35 °C over three successive 12 h periods. Prior to each warming period, KrF_2 was condensed into the reactor at −196 °C, 0.0740 g (0.608 mmol), 0.0593 g (0.487 mmol), and 0.0330 g (0.271 mmol), respectively. Only $TcOF_5$ and a small amount of unreacted $TcO_2F_4^-$ were observed by ^{19}F NMR and Raman spectroscopy.

An attempt was also made to fluorinate TcO_2F_3 to $TcOF_5$ in molten XeF_6. In the drybox, 0.0732 g (0.390 mmol) of TcO_2F_3 was loaded into a T-shaped reaction vessel constructed of $^1/_4$-in. o.d. FEP tubing and fitted with a Kel-F valve. An 8-fold excess of XeF_6 (0.7730 g,

(62) Atomic Energy Control Board (Canada) Radioisotope Safety Poster INFO-0142−1/Rev. 2, Rules for Working with Radioisotopes in a Basic Laboratory.
(63) Bezmel'nitsyn, V. N.; Legasov, V. A.; Chaivanov, B. B. *Proc. Acad. Sci. USSR* **1977**, *235*, 365; *Dokl. Akad. Nauk SSSR* **1977**, *235*, 96.
(64) Malm, J. G.; Chernick, C. L. *Inorg. Synth.* **1966**, *8*, 258.
(65) Mercier, H. P. A.; Sanders, J. C. P.; Schrobilgen, G. J.; Tsai, S. S. *Inorg. Chem.* **1993**, *32*, 386.
(66) Emara, A. A. A.; Schrobilgen, G. J. *Inorg. Chem.* **1992**, *31*, 1323.
(67) Casteel, Jr., W. J.; Kolb, P.; LeBlond, N.; Mercier, H. P. A.; Schrobilgen, G. J. *Inorg. Chem.* **1996**, *35*, 929.
(68) Gillespie, R. J.; Netzer, A.; Schrobilgen, G. J. *Inorg. Chem.* **1974**, *13*, 1455.
(69) Gerken, M.; Schrobilgen, G. J. *Inorg. Chem.* **2000**, *39*, 4244.

3.152 mmol) was condensed onto TcO_2F_3 at −196 °C and pressurized to 1 atm with dry nitrogen. The mixture was warmed to 35 °C, whereupon a yellow-orange solution formed, and the reaction mixture was heated for 5 h. The sample was cooled to −196 °C, evacuated, and warmed to room temperature, whereupon a colorless volatile fraction was condensed into the sidearm of the reactor and an involatile pale yellow solid remained in the other reactor arm. Raman spectroscopy showed that the volatile material was XeF_6 and the involatile fraction was $[Xe_2F_{11}][TcO_2F_4]$. Raman frequencies (cm^{-1}) and intensities for $[Xe_2F_{11}][TcO_2F_4]$ recorded at −80 °C follow and are in good agreement with the previously reported $Xe_2F_{11}^+$ cation frequencies[70] and $TcO_2F_4^-$ frequencies:[7] $TcO_2F_4^-$, 961 (100), 944 (64), 649 (75)/653 (56) sh, 625 (11)/617 (18), 560 (5), 401 (8) sh/406 (10), 321 (20)/328 (11) sh, 302 (5) sh, 234(4), 185 (4), 149 (2); $Xe_2F_{11}^+$: 675 (23), 664 (16), 649 (75)/653 (56) sh, 634 (12), 625 (11), 610 (9), 584 (46) sh/587 (72) sh/591 (91), 416 (4), 401 (8) sh/406 (10), 358 (5), 302 (5) sh, 255 (3); lattice modes, 125 (2), 111 (2), 106 (2), 94 (2), 90 (2), 73 (2) sh, 68 (4).

Preparation of $[Tc_2O_2F_9][Sb_2F_{11}]$ and Crystal Growth. In a drybox, 0.1040 g (0.582 mmol) of SbF_3 was loaded into a $^1/_4$-in. o.d. FEP reactor fitted with a Kel-F valve. Anhydrous HF (ca. 0.5 mL) was condensed onto the solid, and the reactor was pressurized with 1100 Torr of fluorine. The solution was sonicated for 90 min until reaction was complete and SbF_3 had completely dissolved. An HF solution containing 0.133 mmol of $TcOF_5$ was then distilled into the SbF_5/HF reactor at −196 °C through an FEP Y-piece. A bright yellow solid was formed under a pale yellow solution upon warming to room temperature. The solvent and excess SbF_5 were then removed under dynamic vacuum at room temperature through an FEP U-trap at −196 °C, yielding a bright yellow, free-flowing powder after 24 h. Single crystals were grown by dissolving 0.0101 g of $[Tc_2O_2F_9][Sb_2F_{11}]$ in ca. 0.3 mL of anhydrous HF at room temperature in the vertical arm of a $^1/_4$-in. o.d. FEP T-reactor pressurized with 1000 Torr of dry nitrogen. The saturated supernatant was decanted into the horizontal arm of the reactor, and the vertical portion was immersed in an ice/water bath. Deep orange rod-shaped crystals formed after 3 days, and the remaining solution was carefully decanted from the crystals before the solvent was removed under dynamic vacuum at room temperature through an FEP U-trap at −196 °C for 24 h. The reactor was then transferred into a drybox, where single crystals were selected under a microscope and individually sealed inside glass Lindemann capillaries (0.1−0.5 mm i.d.). The crystal used for the data acquisition had the dimensions 0.22 × 0.20 × 0.07 mm^3.

Attempted Preparation of $[TcF_6][AsF_6]$ and Preparation of $[Tc_2O_2F_9][AsF_6]$. An HF solution of $TcOF_5$ (0.0392 g, 0.187 mmol) was prepared in a $^1/_4$-in. o.d. FEP reactor connected to a 316 stainless steel Whitey ORF2 valve by means of a stainless steel $^1/_4$-in. AN nipple. Krypton difluoride (0.2310 g, 1.904 mmol) was condensed into the reactor from an FEP weighing vessel followed by 0.934 mmol of AsF_5. The reaction mixture was warmed to room temperature for a few seconds to achieve complete dissolution of the solids. The solution was then maintained at 0 °C, where gas evolution occurred at a reasonable rate. After 30 min, no obvious change was noted in the color of the solution. The noncondensable gases were removed at −196 °C, and upon warming to 0 °C a yellow solid precipitated from the solution. The reaction was allowed to proceed for a further 2 h until gas evolution ceased, at which point a large amount of yellow solid was present under a pale yellow supernatant. The solvent and excess AsF_5 were then removed at −78 °C by pumping for 18 h through an FEP U-trap cooled to −196 °C for 18 h, yielding a free-flowing yellow powder which was identified by Raman spectroscopy as $[Tc_2O_2F_9][AsF_6]$.

X-ray Crystallography. Collection and Reduction of X-ray Data. The data sets for $TcOF_5$ and $[Tc_2O_2F_9][Sb_2F_{11}]$ were collected with the program SMART[71] on a P4 Siemens diffractometer equipped with a Siemens SMART 1K CCD area detector and a rotating anode with graphite-monochromated Mo Kα radiation (λ = 0.710 73 Å). The diffraction data collection consisted of a full ψ rotation at $\chi = 0°$ using (1200 + 50) 0.3° frames, followed by a series of short (100 frames) ω scans at various χ and ψ settings to fill the gaps. The detector was located at 3.991 cm from the crystal, and a complete data set was acquired at a 2θ setting of 330°. A complete sphere of data was collected, to better than 0.8 Å resolution. The data were reduced with the program SAINT,[71] which applied Lorentz and polarization corrections to the three-dimensionally integrated diffraction spots. The program SADABS[72] was used for the scaling of the diffraction data and the application of an empirical absorption correction based on redundant reflections.

Solution and Refinement of the Structure. The XPREP program[73] was used to confirm the unit cell dimensions and the crystal lattice. The experimental values for $[Tc_2O_2F_9][Sb_2F_{11}]$ when differing from those of $TcOF_5$ are given in square brackets. The solutions were obtained by using Patterson methods, which located the positions of the heavy atoms. Successive difference Fourier syntheses revealed the positions of the remaining oxygen and fluorine atoms. The final refinement was obtained by introducing anisotropic parameters for all the atoms and a weight factor ($w = 1/[\sigma^2(F_o^2) + (0.0358P)^2 + 10.20P]$ [$w = 1/[\sigma^2(F_o^2) + (0.0630P)^2]$]) and gave rise to a residual, R_1, of 0.0256 ($wR_2 = 0.0730$) [$R_1 = 0.0368$ ($wR_2 = 0.0896$)]. In the final difference Fourier map, the maximum and the minimum electron densities were +0.55 and −0.50 [+2.29 and −1.14] $eÅ^{-3}$.

Calculations were performed on a Silicon Graphics model 4600PC workstation with the SHELXL[73] package for structure determination, refinement, and molecular graphics.

Nuclear Magnetic Resonance Spectroscopy. The NMR spectra of all samples were recorded unlocked (field drift < 0.1 Hz h^{-1}). With the exception of the ^{19}F and ^{99}Tc spectra of $TcOF_5$ in SbF_5 solvent, which were recorded on a Bruker DRX-500 spectrometer (11.7438 T; conditions and parameters given in square brackets), all other spectra were recorded on a Bruker AC-300 (7.0463 T) spectrometer equipped with an Aspect 3000 computer. In the latter case, the ^{19}F spectra were acquired with a 5 mm $^1H/^{13}C/^{31}P/^{19}F$ combination probe. In the former case, a 5 mm $^1H/^{19}F$ combination probe was used. The ^{99}Tc spectra were obtained using 10 mm broad-band VSP probes tunable over the range 14−121 [23−202] MHz. The ^{19}F (282.409 MHz) [470.554 MHz] spectra were recorded using a ∼90° pulse width of 7 [2.5] μs. A total of 200 [800] transients were acquired in 32 [64] K memories using a spectral width setting of 25 [100] kHz, an acquisition time of 1.311 [0.328] s, a resolution of 0.77 [1.53] Hz/data point, and a line broadening of 1 [0] Hz. The ^{99}Tc (67.555 MHz) [112.571 MHz] spectra were recorded using a ∼90° pulse width of 9 [10] μs. A total of 2000 [1000] transients were acquired in 16 [32] K memories using a spectral width setting of 50 [100] kHz, an acquisition time of 0.164 [0.164] s, a resolution of 6.10 [3.05] Hz/data point, and a line broadening of 10 [2] Hz. The ^{19}F and ^{99}Tc NMR spectra were referenced to external samples of neat $CFCl_3$ and 0.210 M aqueous $[NH_4][TcO_4]$, respectively, at 30 °C.

NMR samples were prepared and heat sealed under dynamic vacuum at −196 °C in either 4 mm o.d. (^{19}F NMR spectra) or $^1/_4$-in. o.d. (^{99}Tc NMR spectra) FEP sample tubes that had been vacuum-dried and passivated with 1000 Torr of fluorine for a minimum of 12 h prior to use. The ^{19}F and ^{99}Tc NMR spectra of $TcOF_5$ dissolved in neat SbF_5 were obtained on a $^1/_4$-in. o.d. FEP.

Raman Spectroscopy. Raman spectra were recorded as previously described.[12,67] The 514.5 nm line of an Ar^+ ion laser (Spectra-Physics model Stabilite 2016) was used for excitation of the $[Tc_2O_2F_9][Sb_2F_{11}]$ and $[Tc_2O_2F_9][AsF_6]$ samples, and the 647.1 nm line of a Kr^+ ion laser (Lexel model 3500) was used for excitation of the $TcOF_5$ samples. The spectra of all samples except that of $[Tc_2O_2F_9][Sb_2F_{11}]$ were recorded in $^1/_4$-in. or 4 mm o.d. FEP tubes. The spectrum of $[Tc_2O_2F_9][Sb_2F_{11}]$ was recorded on the randomly orientated single crystal used for the X-ray structure determination, but was identical to that obtained for a microcrystalline sample in FEP. All spectra were recorded using the macrosampling chamber of the instrument except the spectra of

(70) Žemva, B.; Jesih, A. *J. Fluorine Chem.* **1984**, *24*, 281.
(71) SMART and SAINT, Release 4.05, Siemens Energy and Automation Inc., Madison, WI, 1996.
(72) Sheldrick, G. M. SADABS (Siemens Area Detector Absorption Corrections), personnal communication, 1996.
(73) Sheldrick, G. M. SHELXTL-Plus, Release 5.03, Siemens Analytical X-ray Instruments Inc., Madison, WI, 1994.

$[Tc_2O_2F_9][Sb_2F_{11}]$ and $TcOF_5$ at room temperature, which were recorded using the microscope optics of the instrument as previously reported.[12] The laser powers at the sample were approximately 300 mW for Ar^+ and 150 mW for Kr^+ using the macrochamber and 10 mW using the microscope optics. Spectral resolutions were 1 cm^{-1} except that for $[Tc_2O_2F_9][Sb_2F_{11}]$, which was 0.5 cm^{-1}. A total of 10 reads having 30 s integration times were summed for each of the Raman spectra except for that of $TcOF_5$ at −150 °C, which used 45 s integration times. The Raman spectrometer was frequency calibrated using the 1018.3 cm^{-1} line of neat indene.

Infrared Spectroscopy. The FT-infrared spectrum was recorded on a BIO-RAD FTS-40 spectrometer at ambient temperature using a cylindrical (10 cm path length, 19 mm o.d., 16 mm i.d) FEP gas cell equipped with AgCl windows, sealed onto the cell body with Kel-F wax (Halocarbon, Hackensack, NJ), a Kel-F valve, and a coldfinger. The spectrum was acquired at 1−2 Torr in 32 scans with a resolution of 8 cm^{-1} and a 5 kHz scan speed. The background, which was recorded prior to spectral acquisition, was subtracted.

Computational Results. All calculations, except for the GIAO calculations, were done with the density functional theory program DGauss[74−76] on SGI computer systems. For the DZVP Tc calculations, the basis set[77] for O and F was of the form (621/41/1) (DZVP) with a (7/3/3) fitting set, and for Tc, the basis set had the form (633321/53211/531) with a fitting basis set of the form (10/5/5). For the TZ94P Tc calculations, a slightly larger basis set[78] of the form (7111/411/1) for O and F with a (7/3/3) fitting basis set was used with a (6333111/531111/5311/1) basis set and a fitting basis set of the form (11/6/5) for Tc. The calculations on the Os and Re compounds were done with the Hay−Wadt ECP and basis sets,[79] the fitting sets in UniChem for Os and Re,[78] and the DZVP2 basis set[77] on O and F. All calculations were done at the local level with the potential fit of Vosko, Wilk, and Nusair.[80] The geometries were optimized by using analytic gradient methods, and second derivatives were also calculated analytically.[81] The NMR chemical shifts were calculated[57] at the local level with the IGLO[54] and LORG[55] approaches to treat the gauge invariance problem.

Additional NMR calculations on $TcOF_5$ and $ReOF_5$ using the GIAO approach for treating the origin problem[56] were done with the program Gaussian94 on SGI computer systems.[82] These calculations were done at the local level with a large basis set denoted as TZ2PF. The basis set for the NMR calculations is of triple-ζ form[83] for O and F augmented by two sets of d polarization functions, each formed from two Gaussian functions and an f polarization function. The Tc basis set is from Huzinaga's compilation[84] and has the form (433331/43311/4211/1).

Acknowledgment. We thank the donors of the Petroleum Research Fund, administered by the American Chemical Society, for support of this work under ACS-PRF Grant No. 31198-AC3. We also thank the Natural Sciences and Engineering Research Council of Canada for the award of graduate scholarships to N.L. The density functional theory calculations were performed under the auspices of the Office of Basic Energy Sciences, U.S. Department of Energy, under Contract DE-AC06-76RLO 1830 with the Battelle Memorial Institute, which operates the Pacific Northwest National Laboratory, a multiprogram national laboratory operated for the Department of Energy. Also gratefully acknowledged are Michael Gerken for recording the ^{19}F and ^{99}Tc NMR spectra on the Bruker DRX-500 spectrometer and Prof. Karl O. Christe for his comments and suggestions relating to the ab initio force constant analyses of MOF_5 (M = Tc, Re, Os).

Supporting Information Available: Unit cell diagram for $[Tc_2O_2F_9][Sb_2F_{11}]$, correlation diagrams for the vibrational modes of $TcOF_5$ and $[Tc_2O_2F_9][Sb_2F_{11}]$, a table of observed and calculated (LDFT) geometric parameters, Mayer bond orders, atomic charges and Mayer valencies for $Re_2O_2F_9^+$, and an X-ray crystallographic file in CIF format for the structure determinations of $TcOF_5$ and $[Tc_2O_2F_9][Sb_2F_{11}]$. This material is available free of charge via the Internet at http://pubs.acs.org.

IC991397E

(74) Andzelm, J.; Wimmer, E.; Salahub, D. R. In *The Challenge of d and f Electrons: Theory and Computation*; Salahub, D. R., Zerner, M. C., Eds.; ACS Symposium Series, No. 394, American Chemical Society: Washington DC, 1989; p 228.
(75) Andzelm, J. In *Density Functional Theory in Chemistry*; Labanowski, J., Andzelm, J., Eds.; Springer-Verlag: New York, 1991; p 155.
(76) Andzelm, J. W.; Wimmer, E. *J. Chem. Phys.* **1992**, *96*, 1280. DGauss is a density functional program which is part of UniChem and is available from Oxford Molecular. Versions 4.1 and 5.0 Beta were used.
(77) Godbout, N.; Salahub, D. R.; Andzelm, J.; Wimmer, E. *Can. J. Chem.* **1992**, *70*, 560.
(78) Lee, C.; Chen, H. Unpublished results. See the UniChem manual, version 3.0.
(79) Hay, P. J.; Wadt, W. R. *J. Chem. Phys.* **1985**, *82*, 270, 284, 299.
(80) Vosko, S. H.; Wilk, L.; Nusair, M. *Can. J. Phys.* **1980**, *58*, 1200.
(81) Komornicki, A.; Fitzgerald, G. *J. Phys. Chem.* **1993**, *98*, 1398 and references therein.
(82) Gaussian 94: Frisch, M. J.; Trucks, G. W.; Schlegel, H. B.; Gill, P. M. W.; Johnson, B. G.; Robb, M. A.; Cheeseman, J. R.; Keith, T. A.; Petersson, G. A.; Montgomery, J. A.; Raghavachari, K.; Al-Laham, M. A.; Zakrzewski, V. G.; Ortiz, J. V.; Foresman, J. B.; Cioslowski, J.; Stefanov, B. B.; Nanayakkara, A.; Challacombe, M.; Peng, C. Y.; Ayala, P. Y.; Chen, W.; Wong, M. W.; Andres, J. L.; Replogle, E. S.; Gomperts, R.; Martin, R. L.; Fox, D. J.; Binkley, J. S.; Defrees, D. J.; Baker, J.; Stewart, J. J. P.; Head-Gordon, M.; Gonzalez, C.; Pople, J. A., Gaussian, Inc., Pittsburgh, PA, 1995.
(83) Dunning, T. H., Jr. *J. Chem. Phys.* **1971**, *55*, 716.
(84) Huzinaga, S.; Andzelm, J.; Klobukowski, M.; Radzio-Andzelm, E.; Sakai, Y.; Tatewaki, H. *Gaussian Basis Sets for Molecular Calculations*; Physical Sciences Data 16; Elsevier: Amsterdam, 1984.